

ORIGINAL RESEARCH ARTICLE

Inducible Pluripotent Stem Cell–Derived Cardiomyocytes Reveal Aberrant Extracellular Regulated Kinase 5 and Mitogen-Activated Protein Kinase Kinase 1/2 Signaling Concomitantly Promote Hypertrophic Cardiomyopathy in *RAF1*-Associated Noonan Syndrome

BACKGROUND: More than 90% of individuals with Noonan syndrome (NS) with mutations clustered in the CR2 domain of *RAF1* present with severe and often lethal hypertrophic cardiomyopathy (HCM). The signaling pathways by which NS *RAF1* mutations promote HCM remain elusive, and so far, there is no known treatment for NS-associated HCM.

METHODS: We used patient-derived *RAF1*^{S257L/+} and CRISPR-Cas9–generated isogenic control inducible pluripotent stem cell (iPSC)–derived cardiomyocytes to model NS *RAF1*-associated HCM and to further delineate the molecular mechanisms underlying the disease.

RESULTS: We show that mutant iPSC–derived cardiomyocytes phenocopy the pathology seen in hearts of patients with NS by exhibiting hypertrophy and structural defects. Through pharmacological and genetic targeting, we identify 2 perturbed concomitant pathways that, together, mediate HCM in *RAF1* mutant iPSC–derived cardiomyocytes. Hyperactivation of mitogen-activated protein kinase kinase 1/2 (MEK1/2), but not extracellular regulated kinase 1/2, causes myofibrillar disarray, whereas the enlarged cardiomyocyte phenotype is a direct consequence of increased extracellular regulated kinase 5 (ERK5) signaling, a pathway not previously known to be involved in NS. RNA-sequencing reveals genes with abnormal expression in *RAF1* mutant iPSC–derived cardiomyocytes and identifies subsets of genes dysregulated by aberrant MEK1/2 or ERK5 pathways that could contribute to the NS-associated HCM.

CONCLUSIONS: Taken together, the results of our study identify the molecular mechanisms by which NS *RAF1* mutations cause HCM and reveal downstream effectors that could serve as therapeutic targets for treatment of NS and perhaps other, more common, congenital HCM disorders.

Fabrice Jaffré, PhD
Clint L. Miller, PhD
Anne Schänzer, MD
Todd Evans, PhD
Amy E. Roberts, MD
Andreas Hahn, MD
Maria I. Kontaridis, PhD

Key Words: cardiomyopathy, hypertrophic ■ clustered regularly interspaced short palindromic repeats ■ gene editing ■ induced pluripotent stem cells ■ mitogen activated protein kinase kinase ■ RASopathies, Noonan syndrome ■ signaling, extracellular regulated kinase

Sources of Funding, see page 223

© 2019 American Heart Association, Inc.

<https://www.ahajournals.org/journal/circ>

Clinical Perspective

What Is New?

- More than 90% of patients with Noonan syndrome (NS) with a mutation in the CR2 domain of RAF1 exhibit severe hypertrophic cardiomyopathy, for which there is no treatment.
- Using NS RAF1 patient and CRISPR-Cas9n-corrected inducible pluripotent stem cell (iPSC)-derived cardiomyocytes, we recapitulated the NS cardiac phenotype; NS iPSC-derived cardiomyocytes exhibit the same hypertrophy and myofibrillar disarray as observed in hearts of patients with NS.
- Mechanistically, activation of mitogen-activated protein kinase kinase 1/2 (MEK1/2), but not extracellular regulated kinase 1/2, triggers abnormal cardiomyocyte structure; conversely, extracellular regulated kinase 5 (ERK5) mediates increased cell size in NS mutant iPSC-derived cardiomyocytes.
- RNA-sequencing identifies genes dysregulated in NS cardiomyocytes that may underlie hypertrophic cardiomyopathy downstream of MEK1/2 and ERK5.

What Are the Clinical Implications?

- Our work demonstrates that patient inducible pluripotent stem cell-derived cardiomyocytes can be used as a disease modeling platform to delineate the functional mechanisms that underlie cardiac hypertrophy in NS and to subsequently identify novel molecular and genetic therapeutic targets.
- MEK1/2 and ERK5 pathways could serve as novel therapeutic targets to treat hypertrophic cardiomyopathy in patients with NS with RAF1 mutations.
- Elucidation of rare disease mechanisms of hypertrophic cardiomyopathy may unravel and reveal causes of other, more common, idiopathic congenital disorders and hypertrophic diseases.

Noonan syndrome (NS) is a common, autosomal dominant, congenital disease with a frequency of ≈ 1 in 2000 live births. It belongs to the RASopathies family of rare genetic diseases, which also includes NS with multiple lentigines (formerly LEOPARD [lentigines, ECG conduction defects, ocular hypertelorism, pulmonary stenosis, abnormalities of the genitalia, retarded growth, deafness] syndrome), cardio-facio-cutaneous syndrome, and Costello syndrome. As the name implies, RASopathies are caused by germ-line mutations that affect genes along the canonical RAS-mitogen-activating protein kinase (MAPK) pathway. Specifically, NS is caused by gain-of-function mutations in this pathway, particularly in *PTPN11*, *SOS1*, *RAF1* (or *c-RAF*), *KRAS*, *NRAS*, and *BRAF* genes.¹ However, additional mutations in other genes have also been described recently.²

Phenotypically, patients with NS present with craniofacial defects, short stature, bleeding anomalies, and skeletal malformations, as well as a panoply of cardiac defects, the most common of which are atrioventricular septal defects and pulmonary valve stenosis. However, $\approx 15\%$ to 20% of patients with NS, often infants or young children, develop hypertrophic cardiomyopathy (HCM), a life-threatening condition that has no treatment, is associated with sudden death, and often quickly deteriorates into heart failure.³ Indeed, individuals with NS present with HCM at earlier ages than individuals with most other familial or idiopathic congenital heart diseases, often accompanied by congestive heart failure and leading to an $\approx 22\%$ mortality rate by the end of the first year of life.³ Hence, identifying and developing efficient therapeutic options to treat HCM in patients with NS is urgently needed.

The *RAF1* gene, located on chromosome 3, codes for a serine/threonine protein kinase of 648 amino acids and has 3 main regions: a conserved region (CR1) containing a RAS binding domain and a C1 domain, a hinge region (CR2), and a kinase domain (CR3). Wild-type RAF1 (or C-RAF) binds to its target downstream effector, mitogen-activated protein kinase kinase (MEK) 1/2, albeit with reduced affinity compared with other RAF (A-RAF and B-RAF) family members. Thus, RAF1 only modestly activates downstream extracellular regulated kinase (ERK) 1/2 signaling,⁴ suggesting that it may play a critical role in growth factor-dependent modulation of ERK1/2-independent pathways. In line with this, RAF1 has demonstrated kinase-independent functions and serves as a scaffold for ERK1/2 pathway-independent proteins.⁵

Among patients with NS, 8% have a mutation in *RAF1*.⁶ Most clinical features are typical of NS; however, $\approx 73\%$ of patients with *RAF1*-associated NS also exhibit HCM, an atypical characteristic of NS.⁶ The frequency of HCM varies, depending on the location of the mutation. The most common *RAF1* mutation, *RAF1*^{S257L+}, is located in the CR2 region and leads to severe, often lethal, HCM in 90% of cases.⁷

Because NS mutations are gain-of-function mutations, it has been suggested that hyperactivation of the ERK1/2 pathway leads to development of HCM.⁸ However, whether other, *RAF1*-specific, pathways contribute to this process has not yet been considered. There is an unusually high incidence of HCM in patients with *RAF1*-associated NS compared with other NS disease-causing genes in the ERK1/2 pathway. Therefore, NS *RAF1* mutations such as *RAF1*^{S257L+} may trigger HCM via an as yet unidentified ERK1/2-independent pathway. Here, we used *RAF1* patient-specific inducible pluripotent stem cell (iPSC)-derived cardiomyocytes (iCMs), as well as genome editing (CRISPR-Cas9), biochemical, and RNA-sequencing technologies, to elucidate the molecular mechanisms and signaling pathways

by which *RAF1*-associated NS mutations cause HCM. Together, this integrative approach identified novel signaling pathways and promising therapeutic targets for treating NS-associated HCM, as well as other, more common, forms of congenital heart disease.

METHODS

The data, analytical methods, and study materials will be made available to other researchers for the purposes of reproducing the results or replicating the procedures. Interested parties should contact the corresponding authors with any inquiry. Patients, parents, or guardians provided written consent for the use of patients' images.

Pharmacological Inhibitors

Wnt-C59 (No. S7037), trametinib (No. S2673), BIX02189 (No. S1531), and cyclosporin A (No. S2286) were obtained from Selleckchem. PD98059 (No. 1213) and U0126 (No. 1144) were obtained from Tocris Bioscience. Phorbol 12-myristate 13-acetate was purchased from Sigma-Aldrich (No. P8139), and ionomycin was obtained from Cayman Chemical (No. 11932). CHIR99021 was obtained from Stem Cell Technologies (No. 72052).

Cell Culture

Cell cultures were maintained at 37°C and 5% CO₂. Human skin fibroblasts were cultured in DMEM (Thermo Fisher Scientific, No. 11965092) supplemented with 10% FBS and passaged by trypsinization (0.25% trypsin EDTA, Thermo Fisher Scientific, No. 25200056). HEK293 cells were cultured in DMEM high glucose (Life Technologies, No. 11965084) supplemented with 10% FBS (Sigma-Aldrich). Human iPSCs were maintained on Matrigel (human embryonic stem cell-qualified matrix, Corning, No. 354277) with mTeSR1 medium (Stem Cell Technologies, No. 05850). Medium was changed every 24 hours, and iPSC lines were passaged with Accutase (Millipore, No. SCR005) with 5 minutes of incubation at 37°C. For replating iPSCs, mTeSR1 medium was supplemented with the Y27632 ROCK inhibitor (10 μmol/L, Selleckchem, No. S1049).

Derivation of Human Fibroblasts and iPSC Generation

Low-passage skin fibroblasts were obtained from a skin biopsy from a female patient with NS carrying an *RAF1*^{S257L/+} mutation or from a healthy pediatric male individual with informed consent under protocols concerning research with biomaterials approved by the local ethics committee of the medical faculty at the Justus-Liebig-University Giessen, Germany. The NS *RAF1*^{S257L/+} and healthy male pediatric iPSC lines were generated with episomal reprogramming vectors. Electroporation of 1 million dermal fibroblasts (Neon Transfection System, Life Technologies, 1650 V, 3 pulses, 10 milliseconds) was performed to deliver 5 reprogramming factors (*OCT3/4*, *SOX2*, *KLF4*, *L-MYC*, *LIN28*) contained in 3 different vectors (1 μg each, gift from Shinya Yamanaka, Addgene plasmids Nos.

27076, 27078, and 27080). An episomal vector coding for *EBNA1* (1 μg, gift from Shinya Yamanaka, Addgene plasmid No. 37624) was coelectroporated to enhance transfection efficiency and expression from the episomal plasmids. After 2 to 3 weeks of culture in reprogramming medium (Pluriton, Stemgent, No. 00-0070), iPSC clones with an embryonic stem cell morphology were picked manually and cultured further in mTeSR1 medium on Matrigel- (Corning, No. 354277) coated plates. Additional characterization was performed by reverse transcriptase-quantitative polymerase chain reaction (PCR) and immunofluorescence for pluripotent markers, as described in the corresponding methods sections. Karyotyping was performed by Cell Line Genetics.

CRISPR-Cas9 Double-Nickase Genome Editing

To correct the *RAF1*^{S257L/+} mutation directly in the iPSC NS line, we took advantage of the CRISPR double-nickase technology.⁹ We first designed 2 guide RNAs (gRNAs) flanking the mutation site using the MIT Optimized CRISPR Design software and a 90-pb donor single-stranded oligonucleotide (Integrated DNA Technologies) carrying the wild-type or mutant sequence that contains a *SaI* restriction site. Several silent mutations were introduced in the single-stranded oligonucleotide to prevent recutting by CRISPR-Cas9dn. Each gRNA (Table I in the online-only Data Supplement) was cloned in the PX462 V2.0 vector (pSpCas9nBB-2A-Puro V2.0, a gift from Feng Zhang; Addgene plasmid No. 62987) as described previously.¹⁰ Correct insertion of the gRNA was verified by Sanger Sequencing using a U6 primer (Table II in the online-only Data Supplement). The pair of gRNA was first tested in HEK293 cells. The 2 PX462 vectors were transfected with Lipofectamine 3000 (No. L3000008, Life Technologies), and the occurrence of insertions/deletions was detected with the Surveyor Assay (Transgenomic, No. 706025) as described previously.¹⁰ Next, 2 to 3 million NS *RAF1* iPSCs were electroporated (Neon Transfection System, Life Technologies, 1400 V, 1 pulse, 20 milliseconds) with 2.5 μg of each PX462 vector concomitantly with 3 μL of 100 μmol/L single-stranded oligonucleotide. After 24 hours, the medium was changed, and an antibiotic selection was performed for 48 hours with 0.5 μg/mL puromycin. iPSCs were further cultured for 3 to 4 days in mTeSR1 medium, next passaged with Accutase (Millipore, No. SCR005), and reseeded at low density (20 000 to 30 000 cells) in mTeSR1 containing 10 μmol/L Y27632 onto 10-cm Matrigel-coated plates. Medium was changed every day, and 10 to 15 days later, single clones were manually picked and replated on two 96-well plates. After 3 to 4 days of expansion in mTeSR1 medium, DNA was extracted with QuickExtract DNA Extraction Solution (Epicentre, No. QE09050). To screen individual clones for correction or introduction, we performed a restriction fragment length polymorphism. To screen for correction, introduction, or occurrence of insertions/deletions, a 402-bp DNA region around the mutation site was PCR-amplified with specific primers (Table II in the online-only Data Supplement). The purified PCR products (Qiagen, QIAquick PCR purification kit No. 28104) were next digested overnight at 37°C with *SaI* restriction enzyme. The digested PCR products were electrophoresed on 2% agarose gels, and clones with a single PCR product were sent for Sanger sequencing

(GENEWIZ). We selected several unmodified clones, clones with the mutation corrected or introduced (resulting from homology-directed repair), but also clones containing insertions/deletions resulting from nonhomologous end joining to generate knockout *RAF1* iPSC lines.

Cardiomyocyte Differentiation

Cardiomyocyte differentiation was induced as previously reported with minor modifications.¹¹ Briefly, iPSC lines were detached using Accutase and seeded as single cells in mTeSR1 medium containing 10 $\mu\text{mol/L}$ Y27632 onto Matrigel-coated plates (1 million/60-mm plate or 2 million/100-mm plate) and cultured for 3 to 4 days in mTeSR1 until they reached 90% confluency. To induce cardiac differentiation of iPSCs (day 0), the medium was changed with RPMI (RPMI-1640, No. 11875085, Life Technologies) containing 6 $\mu\text{mol/L}$ CHIR99021 (Stem Cell Technologies, No. 72052) for 24 hours. On day 1, medium was changed to RPMI+B27 minus insulin (B27 without insulin, No. A1895601, Life Technologies) for 2 days. On day 3, the culture medium was subsequently replaced with RPMI+B27 minus insulin containing 2 $\mu\text{mol/L}$ Wnt-C59 (Selleckchem, No. S7037) for 2 days. From days 5 to 7, the culture medium was replaced with RPMI+B27 minus insulin. On day 7, the medium was changed with RPMI+B27 supplement containing insulin (Life Technologies, No. 17504044) for 2 days. Culture medium was refreshed every 2 days with similar medium.

iCM Purification By DL-Lactate Supplementation

We purified our cultures by performing a DL-lactate supplementation. Briefly, on days 12 to 15, the medium was changed to RPMI without glucose (Life Technologies, No. 11879020) containing 5 mmol/L sodium DL-lactate (Sigma-Aldrich, No. 4263), 213 $\mu\text{g/mL}$ L-ascorbic acid (Sigma-Aldrich, No. A4403), and 500 $\mu\text{g/mL}$ human albumin (Sigma-Aldrich, No. A9731). Medium was changed every 2 days, and after 4 days of DL-lactate supplementation, the beating cardiomyocytes were thereafter maintained in RPMI+B27 supplement or RPMI+10% FBS. Hence, we were able to obtain highly pure cardiomyocyte cultures, with >90% cardiomyocytes at day 20.

Passage of iCMs

At day 20, 60-mm or 10-cm dish iCM cultures were incubated with 1 to 2 mL trypsin-EDTA (Thermo Fisher Scientific, No. 25200056) for 5 minutes at 37°C. To individualize iCMs, cells were pipetted 10 times with a 1-mL pipette tip and transferred onto 1 mL RPMI supplemented with 20% FCS. iCMs were counted and reseeded on 0.1% gelatin-coated plates. For Western blot analysis and RNA extraction, 750 000 to 1 million cells were plated in each well of a 6-well plate. For immunofluorescence imaging, 40 000 iCMs were plated onto 60-mm glass-bottom dishes (MatTek, No. P35G-1.5-14-C).

Western Blots

Cells were lysed in RIPA buffer containing protease and phosphatase inhibitors (Pierce, No. 88668) for 10 minutes on ice. Lysates were collected and cleared by centrifugation at 12 000g for 10 minutes at 4°C. Protein concentration was

determined with the BCA protein assay kit (Pierce, No. 23227). Samples containing 10 to 50 μg protein were separated by SDS-PAGE (Thermo Fisher Scientific, Bolt 10% Bis-Tris Plus mini-gels, No. NW00100BOX) and transferred to polyvinylidene fluoride membranes (Millipore, No. IPVH00010). Membranes were blocked with 5% milk or 5% BSA in TBS-Tween 20 for 1 hour at room temperature and probed with primary antibodies overnight at 4°C. Adequate secondary horseradish peroxidase antibodies were incubated at room temperature for 1 hour. A detailed list of primary antibodies used in this study for Western blot is available in [Table III in the online-only Data Supplement](#). Western blot images were analyzed with the AlphaView software (Cell Biosciences).

Statistical Analysis

The experiments were not randomized, and no statistical method was used to predetermine sample size. The investigators were not blinded to allocation during experiments and outcome assessment. Data were expressed as mean \pm SEM. All experiments are an average of at least 3 independent experiments, and for cell number, surface area, or organized myofibrils calculation in immunostaining assays, 200 to 300 cells per sample were counted for each independent experiment. Statistical analyses were performed with GraphPad Prism 7.01 software. An unpaired 2-tailed Student *t* test was used to calculate significant differences between 2 groups. When >2 groups were compared, 1-way ANOVA was used, followed by the Tukey post hoc honestly significant difference test. A value of $P<0.05$ was considered statistically significant. For reverse transcriptase–quantitative PCR data, an unpaired 2-tailed Student *t* test was used to calculate significant ΔCt differences between 2 groups.

A detailed Materials and Methods section is available in the [online-only Data Supplement](#).

RESULTS

RAF1^{S257L/+} Mutation Leads to Severe Obstructive HCM in a Patient With NS

NS-associated *RAF1* mutations have a high frequency of HCM. We recently identified a female pediatric patient diagnosed with NS and carrying the *RAF1*^{S257L/+} mutation (c.770C>T). The pregnancy was complicated by development of polyhydramnion and fetal arrhythmia. The patient with NS was born after 36 weeks of gestation by caesarean section without complication. Some minor abnormalities such as medial epicanthus, low-set ears, deep hairline, right-sided ptosis, and lateralized mamilla were noticeable at birth and during the postnatal follow-up (Figure 1A). Immediately after birth, the ECG revealed atrial arrhythmias ([Figure 1A in the online-only Data Supplement](#)), which required treatment with atenolol. Echocardiogram confirmed a biventricular obstructive HCM, but genetic testing was not performed at that time. However, septal hypertrophy worsened within the next year, resulting in

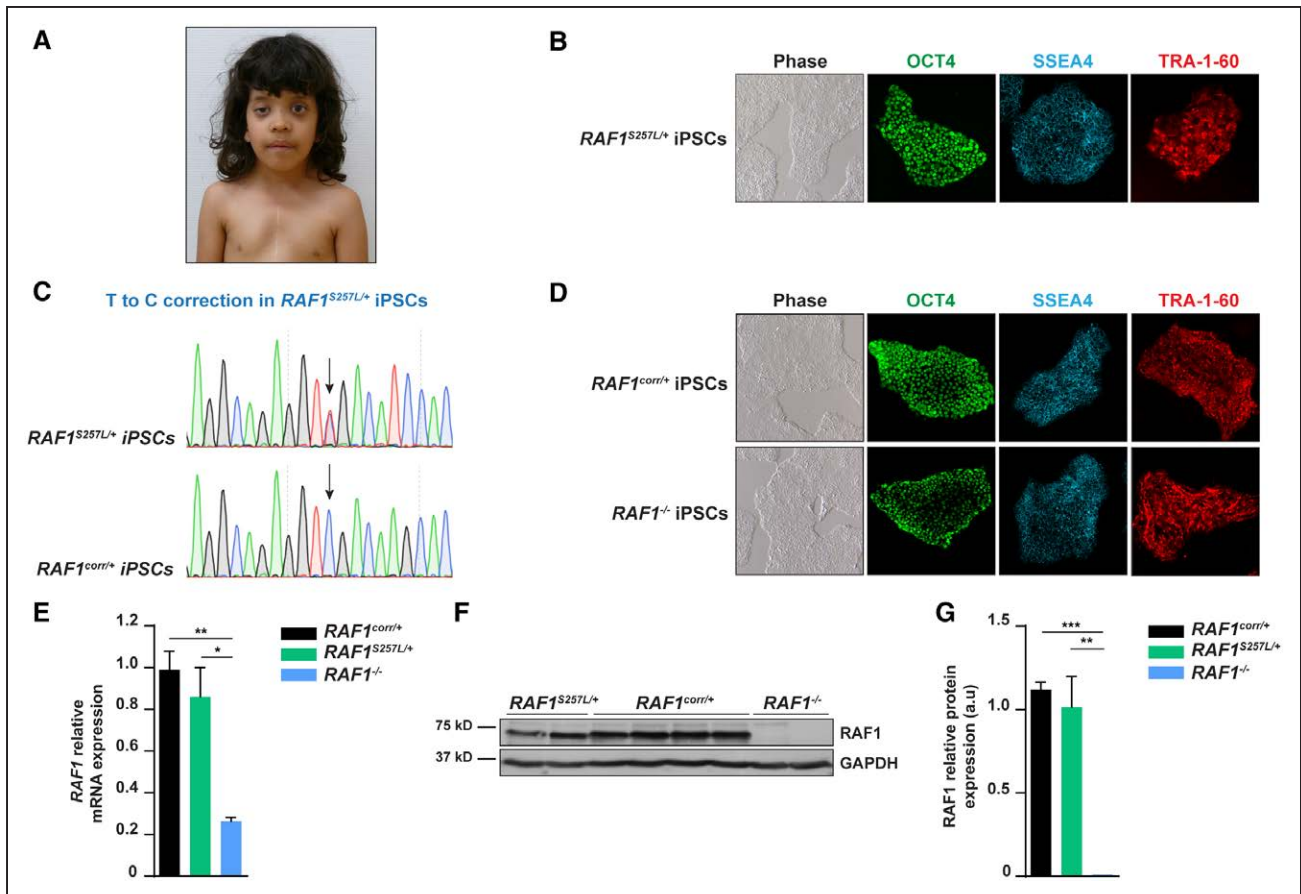


Figure 1. Generation of Noonan syndrome (NS) $RAF1^{S257L/+}$ inducible pluripotent stem cells (iPSCs) and mutation correction using CRISPR-Cas9dn genome editing.

A, A patient with NS at 8 years of age showing right-sided ptosis, medial epicanthus, low-set ears, deep hairline, and lateralized mammilla. A thoracic scar is observed as the consequence of a myectomy performed at 5 years of age. Written consent was obtained from the patient's family for publication of the image. **B**, Phase image and immunofluorescence staining of $RAF1^{S257L/+}$ iPSC colonies for the pluripotency markers OCT4, SSEA4, and TRA-1 to 60. **C**, DNA Sanger sequencing analysis of NS $RAF1^{S257L/+}$ and isogenic corrected $RAF1^{corr/+}$ iPSC lines. **D**, Phase image and immunofluorescence staining of $RAF1^{corr/+}$ and $RAF1^{-/-}$ iPSC colonies for the pluripotency markers OCT4, SSEA4, and TRA-1 to 60. **E**, $RAF1$ mRNA levels in isogenic $RAF1^{corr/+}$, $RAF1^{S257L/+}$, and $RAF1^{-/-}$ iPSC lines detected by reverse transcriptase–quantitative polymerase chain reaction. The mRNA levels were normalized to the expression of GAPDH ($n=3$). **F**, Western blot of $RAF1$ expression in isogenic $RAF1^{corr/+}$, $RAF1^{S257L/+}$, and $RAF1^{-/-}$ iPSC lines. Each lane represents 1 different iPSC clone of each genotype. **G**, Quantification of $RAF1$ protein levels normalized to GAPDH in isogenic $RAF1^{corr/+}$, $RAF1^{S257L/+}$, and $RAF1^{-/-}$ iPSCs. Results are represented as mean \pm SEM. * $P<0.05$. ** $P<0.01$. *** $P<0.001$. a.u. indicates arbitrary units.

obstruction of the left ventricular outflow tract (Table IV in the online-only Data Supplement).

At 5 and one-half years of age, a cardiac catheterization examination revealed cardiac hypertrophy with left ventricular intracavity pressure gradient of 70 mmHg, prompting an immediate transaortic septal myectomy. Histological analyses of the myectomized cardiac tissue showed severe perivascular and endocardial fibrosis, endothelial thickening, and focal accumulation of lymphocytes and granulocytes, primarily in endocardium (arrows; Figure IB.1 through IB.4 in the online-only Data Supplement). Moderate variations in cardiomyocyte size and enlarged nuclei were also apparent, although expression of desmin, a marker for sarcomeric architecture, appeared normal (Figure IB.5 through IB.7 in the online-only Data Supplement). Finally, electron microscopy demonstrated perinuclear mitochondrial aggregates with autophagic vacuoles

containing myelin-like bodies (Figure IB.8 in the online-only Data Supplement).

At 8 years of age, the patient had an afebrile seizure. At that time, short stature was noticed (height, 114 cm; 3 cm less than the third percentile), but no lentigines or other cutaneous symptoms were apparent. NS was therefore suspected because of the conjunction of her craniofacial features (Figure 1A), her short stature, and the obstructive HCM. Genetic testing revealed a S257L⁺ point mutation located in exon 7 of $RAF1$ ($RAF1^{S257L/+}$).

At her last follow-up, at 16 years of age, the patient's cardiac status was stable, as demonstrated by magnetic resonance imaging (Figure IC in the online-only Data Supplement). Her height was 146 cm (5 cm less than the third percentile). The status of this patient's HCM was considered nonprogressive, and at this stage, HCM did not limit daily life activities.

Generation of Human *RAF1*^{S257L/+} iPSCs

To study the molecular consequences of this patient's *RAF1* mutation in human cardiomyocytes, we generated footprint-free iPSCs by electroporating 4 episomal vectors expressing *OCT3/4*, *LIN28*, *SOX2*, *KLF4*, and *L-MYC* into the dermal fibroblasts of the above-mentioned patient with NS-associated *RAF1*^{S257L/+} (Figure 1B). We confirmed pluripotency of the iPSC lines by immunofluorescence (Figure 1B) and mRNA expression of pluripotent markers (Figure IIA in the online-only Data Supplement).

Correction of the NS-Associated *RAF1*^{S257L/+} Mutation and Generation of *RAF1* Knockout iPSCs Using CRISPR-Cas9 Double-Nickase Technology

Lack of genetically matched, nondiseased controls renders interpretation of observed phenotypes in iPSCs difficult to attribute only to the disease-causing mutations. Moreover, different genetic backgrounds between various iPSC lines can confound interpretation of the data. To overcome these issues and to focus specifically on the consequences of the NS-associated *RAF1* mutation, we corrected the iPSC-derived *RAF1*^{S257L/+} mutant cells using CRISPR-Cas9 double-nickase technology (CRISPR-Cas9dn) to generate an isogenic control line (Figure 1C and 1D and Figure IIB in the online-only Data Supplement). CRISPR-Cas9dn allows specific targeting of a genomic locus and, unlike Cas9, generates extremely low off-target events.⁹ Using HEK293 cells, we tested a pair of 20-nucleotide-long gRNAs specific to the targeted region and flanking the mutated site (Figure IIC in the online-only Data Supplement); we observed insertions/deletions only in the cells transfected with both gRNAs (Figure IID in the online-only Data Supplement). We next electroporated the *RAF1*^{S257L/+} iPSCs with both the gRNAs and the single-stranded oligonucleotide repair template (Figure IIC in the online-only Data Supplement). After puromycin selection and restriction fragment length polymorphism-based screening (Figure IIE in the online-only Data Supplement), we obtained several corrected clones (*RAF1*^{corr/+}), as demonstrated by Sanger sequencing (Figure 1C). The mRNA and protein levels of *RAF1* remained unchanged between parental mutant and corrected isogenic iPSC lines (Figure 1E through 1G).

In addition, we leveraged CRISPR-Cas9dn to generate an isogenic *RAF1* knockout line (*RAF1*^{-/-}; Figure 1D). To do this, we selected clones with various genomic insertions/deletions near the mutated site and analyzed the *RAF1* mRNA and protein expression levels in each clone. Several of our selected clones displayed reduced *RAF1* mRNA (Figure 1E) and complete ablation of *RAF1* protein (Figure 1F and 1G), demonstrating that

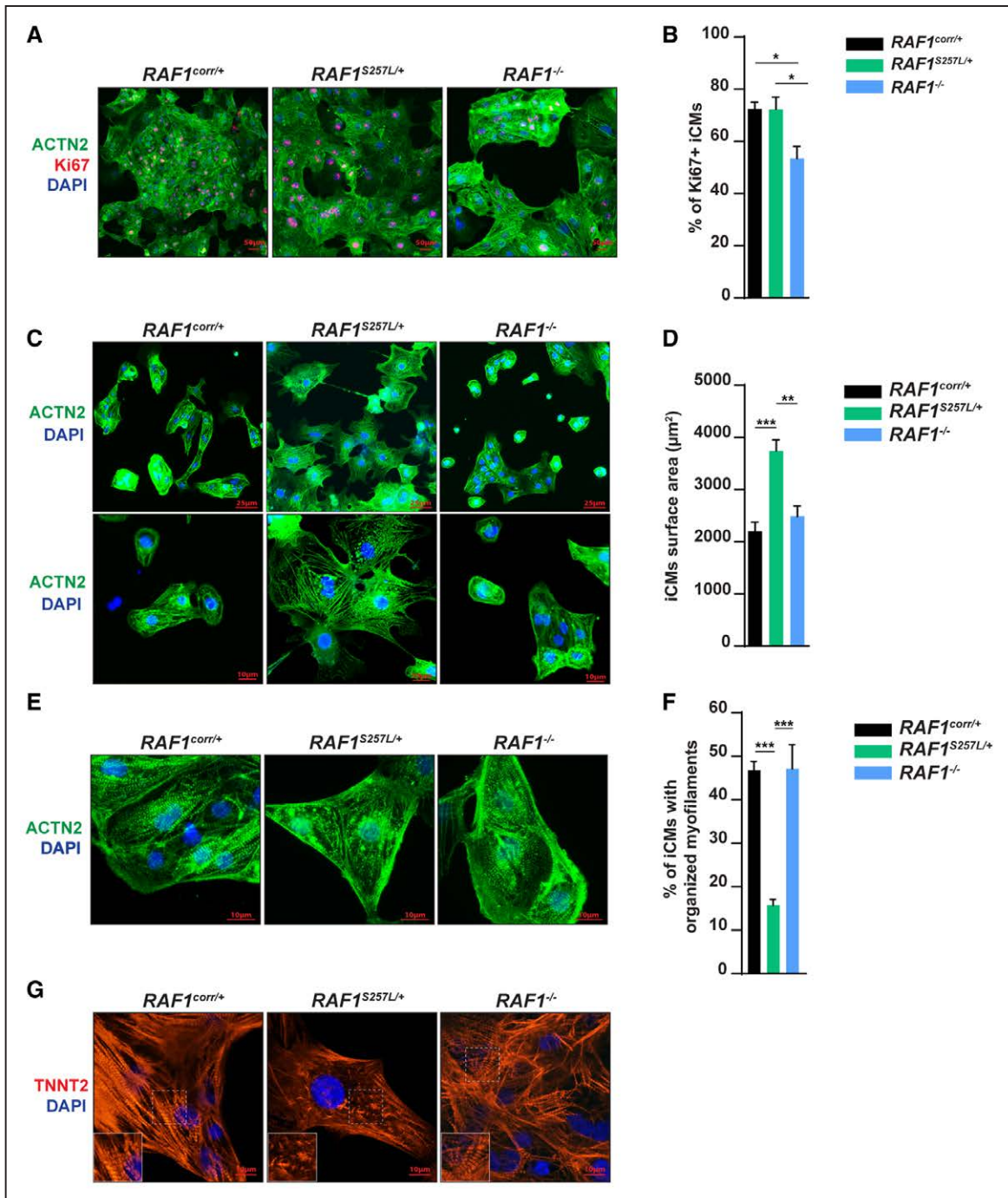
some targeted site deletions lead to mRNA instability and therefore *RAF1*^{-/-} isogenic iPSC lines. Pluripotency and chromosomal integrity of the *RAF1*^{corr/+} or *RAF1*^{-/-} iPSC lines were not impaired, as demonstrated by immunofluorescence and karyotyping analyses, respectively (Figure 1D and Figure IIF in the online-only Data Supplement).

Deletion of *RAF1*, but Not Expression of the *RAF1*^{S257L/+} Mutation, Alters Cardiomyocyte Proliferation

To study the molecular mechanisms underlying HCM in patients with *RAF1*^{S257L/+}, we differentiated isogenic iPSC lines into beating cardiomyocytes (iCMs) using small molecules that modulate GSK3 and Wnt- β -catenin pathways, as previously described¹¹ (Video I in the online-only Data Supplement). After supplementation of the cultures with DL-lactate, we obtained a highly pure population of iCMs (>90%) from all 3 genotypes (*RAF1*^{S257L/+}, *RAF1*^{corr/+}, *RAF1*^{-/-}; Figure III in the online-only Data Supplement). Because the ERK1/2 pathway plays a central role in the proliferation of cardiomyocytes,¹² we next assessed the proliferation rate of *RAF1*^{corr/+}, *RAF1*^{S257L/+}, and *RAF1*^{-/-} iCMs by measuring the number of Ki67-positive iCMs. Proliferation rates of mutant and isogenic control iCMs were comparable (Figure 2A and 2B). However, deletion of *RAF1* reduced iCMs proliferation by 30% (Figure 2B), suggesting that *RAF1* may be necessary for cardiomyocyte proliferation but that its increased kinase activity does not potentiate this process.

iPSC-Derived *RAF1*^{S257L/+} Cardiomyocytes Are Enlarged and Develop Myofibrillar Disarray

To determine whether *RAF1*^{S257L/+} triggers cell-autonomous cardiomyocyte hypertrophy, we measured cell surface area of individual iCMs. *RAF1*^{S257L/+} iCMs exhibited a significant increase in cell surface area (170%) compared with *RAF1*^{corr/+} cells (Figure 2C and 2D and Figure IVA and IVB in the online-only Data Supplement). In contrast, genetic deletion of *RAF1* did not influence iCM cell surface area (Figure 2C and 2D). Next, we investigated the sarcomeric organization of mutant iCMs using ACTN2 immunofluorescence staining as a marker for sarcomeric integrity. Although a high number of *RAF1*^{corr/+} and *RAF1*^{-/-} iCMs showed well-organized striated myofibrils, with a typical pattern of cross-striations that correspond to the Z bands of sarcomeres (Figure 2E and 2F), the *RAF1*^{S257L/+} mutant iCMs displayed significant myofibrillar disarray (Figure 2E and 2F and Figure IVC in the online-only Data Supplement), a typical characteristic of pathophysiology observed in patients



A, Inducible pluripotent stem cell–derived cardiomyocyte (iCM) proliferation assessed by Ki67 immunofluorescence. Percentage of Ki67-positive iCMs (Actinin Alpha 2 [ACTN2]-positive cells) with nuclear DAPI staining. **B**, Quantification of Ki67-positive cells in isogenic *RAF1*^{corr/+}, *RAF1*^{S257L/+}, and *RAF1*^{-/-} iCMs obtained from 4 to 6 independent differentiations. For each independent experiment, 3 immunofluorescence images were taken randomly for each well of each lineage (representing 300–500 cells per lineage for each independent experiment). **C**, Representative immunofluorescence image of isogenic *RAF1*^{corr/+}, *RAF1*^{S257L/+}, and *RAF1*^{-/-} iCMs stained for ACTN2 and DAPI. **D**, Quantification of iCM surface area for each lineage of iCMs obtained from 6 to 10 independent differentiations. For each independent experiment, 7 to 10 immunofluorescence images were taken randomly for each well of each lineage (representing 200–300 iCMs measured per independent experiment). **E**, Representative images of myofibrillar organization in isogenic *RAF1*^{corr/+}, *RAF1*^{S257L/+}, and *RAF1*^{-/-} iCMs shown by immunofluorescence staining for ACTN2 and DAPI. **F**, Quantification of iCMs with organized myofilaments after ACTN2 immunostaining (n=3). For each independent experiment, 7 to 10 immunofluorescence images were taken randomly for each well of each lineage (representing 100–300 iCMs). Results are presented as mean±SEM. **P*<0.05. ***P*<0.01. ****P*<0.001. **G**, Representative confocal images (×63 objective) of myofibrillar organization in isogenic *RAF1*^{corr/+}, *RAF1*^{S257L/+}, and *RAF1*^{-/-} iCMs shown by immunofluorescence staining for troponin T2 (TNNT2) and 4',6-diamidino-2-phenylindole (DAPI).

with NS with HCM.¹³ Moreover, a large number of mutant iCMs showed disorganized α -actinin fibers, with evidence of punctate sarcomeric α -actinin distribution, as well as narrowing and elongation of sarcomeres, as shown by confocal microscopy in cells stained for TNNT2 (Figure 2G and Figure IVD in the online-only Data Supplement) or ACTN2 (Figure IVE in the online-only Data Supplement). Despite this difference in myofibrillar structure, expression of the sarcomeric protein ACTN2 was similar between corrected and *RAF1* mutant iCMs (Figure IVF and IVG in the online-only Data Supplement).

These findings were validated in a second, unrelated iPSC line derived from a healthy pediatric patient. We used CRISPR-Cas9dn to introduce the *RAF1* S257L heterozygous mutation into iPSCs derived from a healthy pediatric individual (*RAF1*^{S257L*intr./+*}; Figure VA through VD in the online-only Data Supplement). Here, we similarly observed enlarged cardiomyocyte cell size (Figure VE and VF in the online-only Data Supplement) and an increased myofiber disarray (Figure VG and VH in the online-only Data Supplement) compared with the isogenic control (*RAF1*^{+/+}) iCMs. These data confirm that *RAF1*^{S257L/+} alone is sufficient to induce the NS-associated features of HCM. The extent to which the mutation induced cell size and myofibrillar disarray was different between the 2 mutant iPSC lines; the HCM phenotype observed in *RAF1*^{S257L*intr./+*} iCMs was less pronounced compared with the *RAF1*^{S257L/+} iCMs in the patient with NS, suggesting that there may be genetic modifiers that contribute to the severity of the disease and that, consequently, using patient-derived iCMs with a monogenic mutation might constitute a better model for studying disease than introducing the mutation in an unrelated iPSC line.

***RAF1*^{S257L/+} iCMs Exhibit Abnormal Relaxation**

We next assayed the contractility at day 30 of the mutant iCMs. *RAF1*^{S257L/+} iCMs had normal amplitude, time to peak, and contraction duration (Figure VIA through VIE in the online-only Data Supplement) but had decreased beating rate and impaired relaxation time (Figure VIA, VIB, VIF, and VIG and Videos II and III in the online-only Data Supplement). These data are indicative of a defect in diastolic relaxation, results that are similarly observed in patients with NS with HCM.¹⁴ Together, these data suggest that the impaired contractility may, at least in part, contribute to the hypertrophic phenotype in *RAF1*^{S257L/+} iCMs.

***RAF1*^{S257L/+} Leads to Increased MEK1/2-ERK1/2 Activity in iCMs**

Dephosphorylation of the RAF1 Ser259 residue is required for initiation of RAF1 activation. In an ectopic

overexpression system, the S257L *RAF1* mutation drastically reduced Ser259 phosphorylation by preventing RAF1 binding to 14-3-3, causing RAF1 to preferentially adopt an open and active conformation.¹⁵ Here, we found that Ser259 phosphorylation was significantly attenuated in *RAF1*^{S257L/+} iCMs (Figure 3A and 3B). In contrast, Ser338, which is phosphorylated by p21 activated kinase 1, was hyperphosphorylated in mutant iCMs (Figure 3A and 3B), suggesting that access to Ser338 is facilitated by the more open conformation of the RAF1 mutant. RAF1 protein expression was similar between *RAF1*^{S257L/+} and *RAF1*^{corr/+} iCMs (Figure 3A and 3B).

In addition, activation of MEK1/2, the only known downstream target of RAF1 and a direct readout of RAF1 kinase activity, was strongly increased in *RAF1*^{S257L/+} iCMs (5-fold over control levels) compared with isogenic corrected control iCMs (Figure 3C and 3D and Figure VIIA in the online-only Data Supplement). Activity of ERK1/2 also increased in *RAF1*^{S257L/+} iCMs, but to a more modest extent (1.8-fold over control level) (Figure 3E and 3F and Figure VIIB in the online-only Data Supplement). Similarly, MEK1/2 activity was increased in *RAF1*^{S257L*intr./+*} iCMs compared with isogenic control cells (Figure VII and VIJ in the online-only Data Supplement). However, unlike in *RAF1*^{S257L/+} iCMs, we did not observe a significant increase in ERK1/2 activity in *RAF1*^{S257L*intr./+*} iCMs, suggesting that, as mentioned previously, introducing a mutation in unrelated iPSC lines may not allow the full recapitulation of the molecular mechanisms underlying a monogenic disease.

Complete ablation of RAF1 did not reduce the baseline activity of either MEK1/2 or ERK1/2 in *RAF1*^{-/-} iCMs (Figure 3C through 3F), suggesting that RAF1 may be dispensable for activation of ERK1/2 in these iCMs. Although not statistically significant, MEK1/2 phosphorylation was slightly increased in *RAF1*^{-/-} iCMs; this is well in line with findings from a previous study that increased MEK1/2 activity in RAF1 knockout mouse embryonic fibroblasts was mediated by increased BRAF (B-Raf proto-oncogene, serine/threonine kinase) activity.¹⁶ Therefore, we next measured BRAF protein levels in our iCMs; we similarly found that BRAF protein expression was slightly increased in the knockout iCMs (but not in the *RAF1*^{S257L/+} iCMs) compared with isogenic control iCMs (Figure VIIC and VIID in the online-only Data Supplement). It is likely that deletion of RAF1 triggers a feedback mechanism that induces BRAF expression in an effort to maintain sufficient levels of ERK1/2 activity and to allow cell survival.

Because of the discrepancy in levels of activation between MEK1/2 and ERK1/2 in *RAF1*^{S257L/+} iCMs, we hypothesized that a feedback loop may also be induced to regulate the hyperactivity of the pathway. Indeed, we found that protein expression of MAPK phosphatase 3 (MKP3), a phosphatase known to specifically target hyper-phosphorylated ERK1/2, was induced in

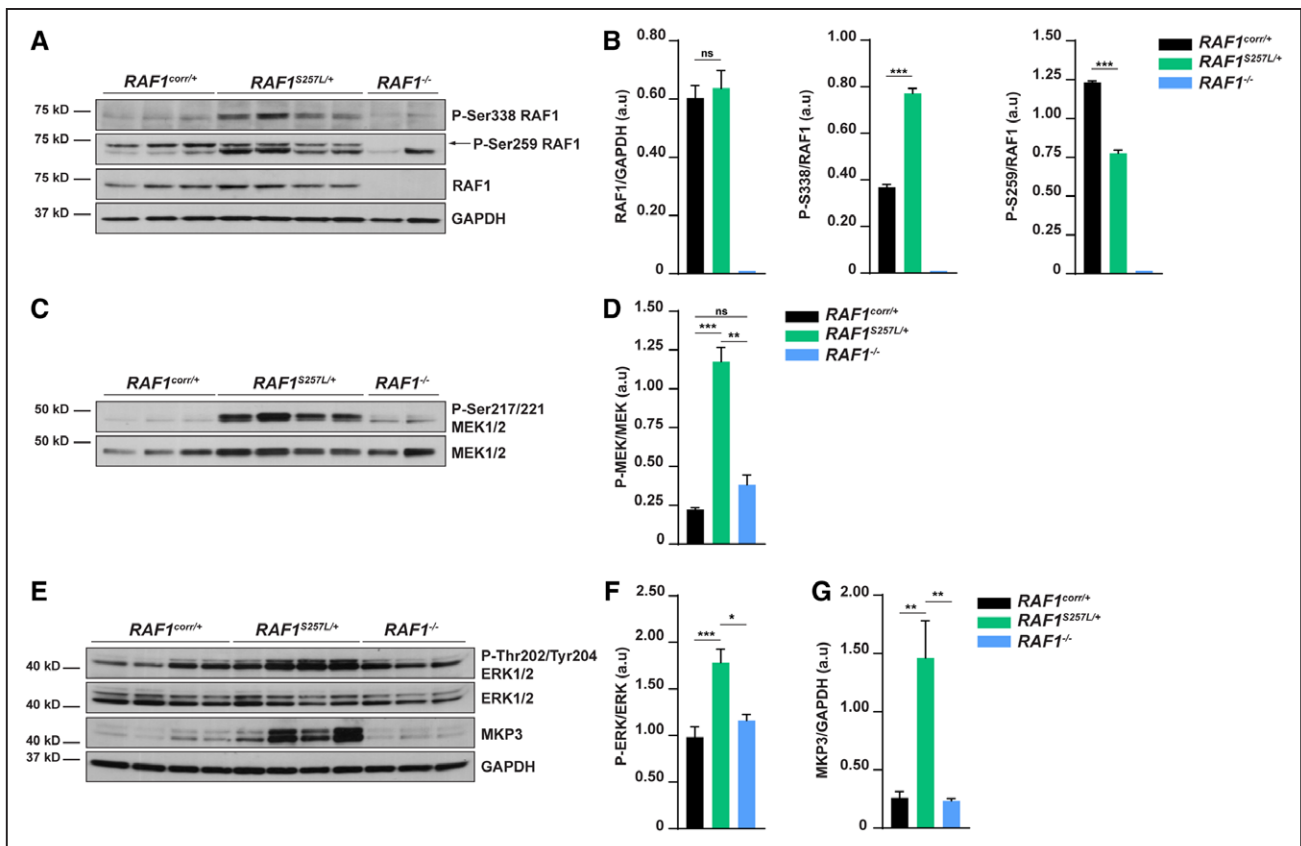


Figure 3. The mitogen-activated protein kinase kinase 1/2 (MEK1/2)–extracellular regulated kinase 1/2 (ERK1/2) pathway is activated in *RAF1*^{S257L/+} cardiomyocytes.

A, Western blots of RAF1, phospho-Ser338 RAF1, and phospho-Ser259 RAF1 in *RAF1*^{corr/+}, *RAF1*^{S257L/+}, and *RAF1*^{-/-} inducible pluripotent stem cell–derived cardiomyocytes (iCMs). **B**, Quantification of RAF1, phospho-Ser338 RAF1, and phospho-Ser259 RAF1 protein levels. RAF1 protein levels were normalized to GAPDH. Phospho-RAF1 levels were normalized to total RAF1 (n=2–4). **C**, Western blots of phospho-MEK1/2 (Ser217/221) and MEK1/2 levels in isogenic *RAF1*^{corr/+}, *RAF1*^{S257L/+}, and *RAF1*^{-/-} iCMs. **D**, Quantification of MEK1/2 activation levels. Phospho-MEK1/2 levels were normalized to total MEK1/2 (n=2–4). **E**, Western blots of phospho-ERK1/2, ERK1/2, MAPK phosphatase 3 (MKP3), and GAPDH levels in isogenic *RAF1*^{corr/+}, *RAF1*^{S257L/+}, and *RAF1*^{-/-} iCMs. **F**, Quantification levels of activated ERK1/2 in isogenic *RAF1*^{corr/+}, *RAF1*^{S257L/+}, and *RAF1*^{-/-} iCMs. Phospho-ERK1/2 (Thr202/Tyr204) levels were normalized to total ERK1/2 (n=3–4). **G**, Quantification of MKP3 protein levels in isogenic *RAF1*^{corr/+}, *RAF1*^{S257L/+}, and *RAF1*^{-/-} iCMs. MKP3 protein levels were normalized to GAPDH. Each lane represents 1 independent differentiation of each lineage. Results are represented as mean±SEM. ns indicates nonsignificant. **P*<0.05. ***P*<0.01. ****P*<0.001. a.u. indicates arbitrary units.

RAF1^{S257L/+} iCMs compared with *RAF1*^{corr/+} or *RAF1*^{-/-} iCMs (5-fold over control or knockout levels; Figure 3E through 3G and Figure VIII E in the online-only Data Supplement).

MEK1/2, but Not ERK1/2, Inhibition Rescues Myofibrillar Disarray but Does Not Prevent Cardiomyocyte Hypertrophy in *RAF1*^{S257L/+} iCMs

To test whether activation of ERK1/2 is responsible for the mutant iCM hypertrophy and structural defects, we treated *RAF1*^{S257L/+} iCMs with 3 different MEK1/2 inhibitors (U0126, PD98059, and trametinib) for 48 hours. As expected, all 3 inhibitors dramatically reduced ERK1/2 phosphorylation in mutant iCMs (Figure 4A and 4B and Figure VIIF in the online-only Data Supplement). Pharmacological suppression of ERK1/2 activity, through inhibition of MEK1/2 activity, led to significantly increased MEK1/2 phosphorylation, likely as a result of

the abrogation of activated ERK1/2–dependent negative feedback mechanisms regulating RAS and RAF activities (Figure 4A and 4B and Figure VIIF in the online-only Data Supplement), as previously shown.¹⁷ Similar results were found in *RAF1*^{corr/+} (Figure VIIIA and VIIIB in the online-only Data Supplement) and isogenic control *RAF1*^{+/+} iCMs, indicating that increased MEK1/2 phosphorylation is a direct result of ERK1/2 inhibition specifically, not a consequence of the NS-associated *RAF1* mutation in iCMs. Strikingly, treatment of *RAF1*^{S257L/+} iCMs with U0126 or trametinib also reduced MEK1/2 protein levels, in addition to inhibiting downstream signaling in *RAF1*^{S257L/+} (Figure 4A and 4B), *RAF1*^{corr/+} (Figure VIIIA and VIIIB in the online-only Data Supplement), and *RAF1*^{+/+} (Figure VIIIC in the online-only Data Supplement) iCMs. This is likely the result of inhibitor-mediated (not mutation-mediated) protein degradation, because MEK1/2 mRNA levels were similar, both in the presence or absence of inhibitor and in the presence or absence of the NS mutation (Figure VIID in the

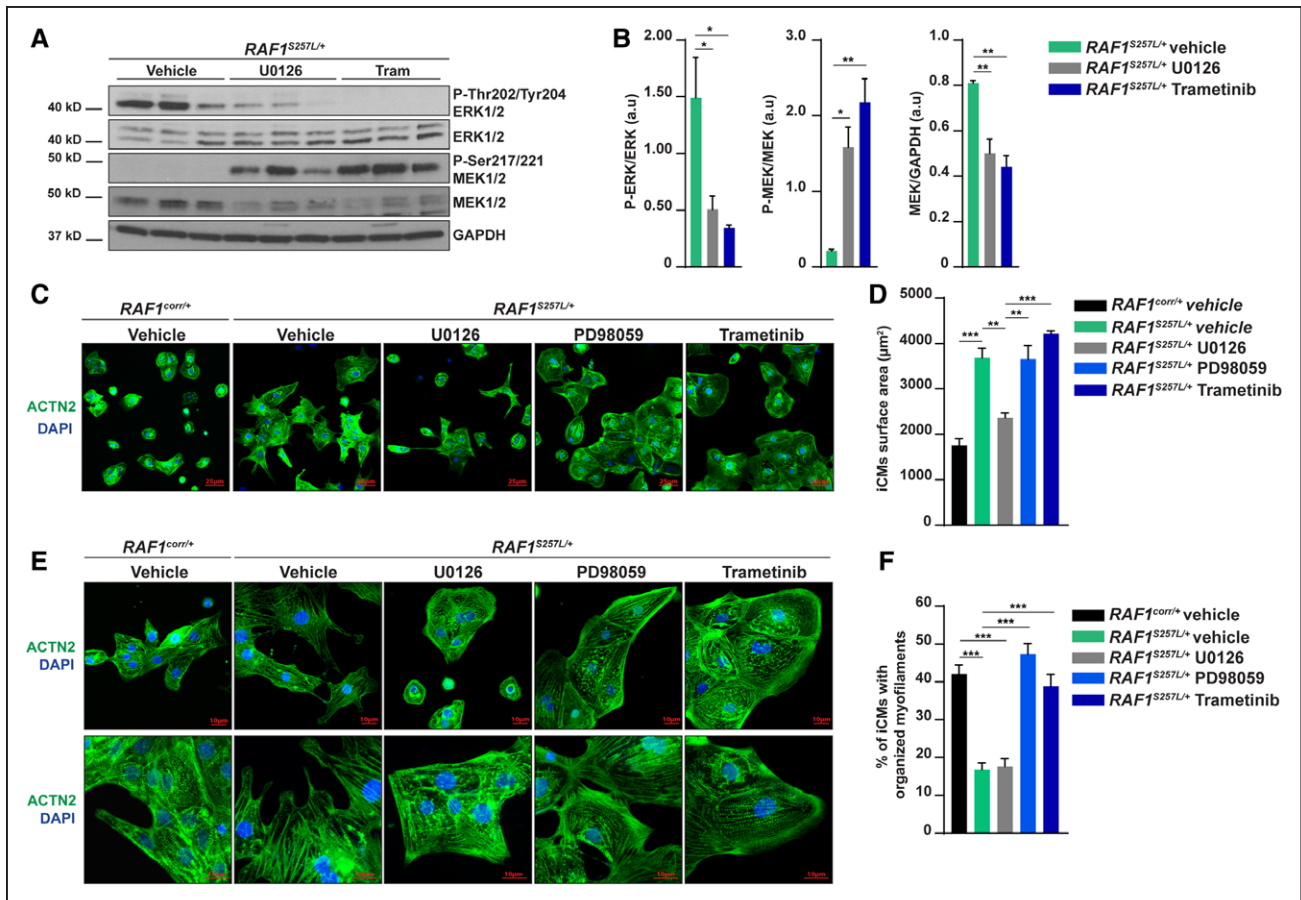


Figure 4. Inhibition of the mitogen-activated protein kinase 1/2 (MEK1/2)–extracellular regulated kinase 1/2 (ERK1/2) pathway does not prevent hypertrophy but rescues structural defects in *RAF1*^{S257L/+} cardiomyocytes.

A, Western blot of phospho-ERK1/2, ERK1/2, phospho-MEK1/2 and MEK1/2 levels in vehicle mutant inducible pluripotent stem cell–derived cardiomyocytes (iCMs) or treated for 48 hours with U0126 (25 µmol/L) or trametinib (Tram; 10 µmol/L). Each lane represents 1 independent differentiation of each lineage. **B**, Quantification of activated levels of ERK1/2 and MEK1/2 and total MEK1/2 protein levels. Phospho-ERK1/2 levels were normalized to total ERK1/2. Phospho-MEK1/2 levels were normalized to total MEK1/2. MEK1/2 protein levels were normalized to GAPDH levels. Representative immunofluorescence images (**C**) and quantification of iCM surface area (**D**) of *RAF1*^{corr/+} vehicle or *RAF1*^{S257L/+} iCMs (Actinin Alpha 2 [ACTN2] and 4',6-diamidino-2-phenylindole [DAPI] positive) vehicle or treated for 48 hours with U0126 (25 µmol/L), PD98059 (25 µmol/L), or trametinib (10 µmol/L). Results were obtained from 3 to 5 independent differentiations (n=3–5). **E**, Representative images of myofibrillar organization and quantification of iCMs with organized myofibrils (**F**) in *RAF1*^{corr/+} vehicle or *RAF1*^{S257L/+} iCM vehicle or treated for 48 hours with U0126 (25 µmol/L), PD98059 (25 µmol/L), or trametinib (10 µmol/L). Results were obtained from 3 independent differentiations (n=3). For each independent experiment, 7 to 10 immunofluorescence images were taken randomly for each well of each condition (representing 200–300 iCMs measured per independent experiment). Results are represented as mean±SEM. **P*<0.05. ***P*<0.01. ****P*<0.001.

online-only Data Supplement). Despite reducing phosphorylation of ERK1/2, MEK1/2 inhibitors did not elicit cell death in mutant cardiomyocytes (Figure IX in the online-only Data Supplement).

Although ERK1/2 activation was strongly reduced, there was no significant effect on hypertrophy in *RAF1*^{S257L/+} iCMs in response to treatment with either PD98059 or trametinib (Figure 4C and 4D), suggesting that MEK1/2-ERK1/2 activation is not the principal driver of hypertrophy in NS-associated *RAF1* mutations. Remarkably, however, inhibition of *RAF1*^{S257L/+} iCMs by these inhibitors resolved the myofibrillar disarray (Figure 4E and 4F), suggesting that proper regulation of MEK1/2 or ERK1/2 signaling is required to maintain the structural integrity of cardiomyocytes. Surprisingly, treatment of *RAF1*^{S257L/+} iCMs with U0126 did, in fact, significantly reduce cell surface area (Figure 4C and 4D),

without having any effect on myofibrillar disarray (Figure 4E and 4F). These data suggest that this inhibitor likely has an additional, MEK1/2-ERK1/2-independent, target required to modulate hypertrophy in *RAF1* mutant iCMs.

PD98059 and trametinib block RAF-dependent activation of MEK1/2, whereas U0126 blocks direct activation of ERK1/2 by MEK1/2.^{18,19} Therefore, to delineate the contribution of MEK1/2 or ERK1/2 on the HCM phenotype, we sought to directly suppress ERK1/2 activity through overexpression of MKP3 in *RAF1*^{S257L/+} iCMs. Using a green fluorescent protein (GFP)–expressing adenovirus, we tested the optimal multiplicity of infection required to infect the majority of mutant iCMs. We found that >90% of *RAF1*^{S257L/+} iCMs were GFP⁺ and overexpressed MKP3 when infected with Ad-GFP or Ad-MKP3, respectively, at a multiplicity of infection of 20

(Figure XA and XB in the online-only Data Supplement). As expected, overexpression of MKP3 in *RAF1^{S257L/+}* iCMs strongly reduced phosphorylation of ERK1/2 compared with cells with GFP expression alone (Figure 5A and 5B). Like the MEK1/2 inhibitors PD98059 and trametinib, targeted inhibition of ERK1/2 activity with Ad-MKP3 did not reduce the increased cell surface area of *RAF1^{S257L/+}* iCMs (Figure 5C and 5D). However, unlike these inhibitors, Ad-MKP3 had no effect on myofiber disarray (Figure 5E and 5F), suggesting that the myofiber abnormalities in the *RAF1^{S257L/+}* mutant iCMs are mediated by MEK1/2, and not ERK1/2, hyperactivity.

Calcineurin–Nuclear Factor of Activated T Cells (NFAT), AKT/Mechanistic Target of Rapamycin (mTOR), p38-MAPK, or c-Jun N-Terminal Kinase (JNK)–MAPK Signaling Is Not Abnormally Regulated and Does Not Mediate Cardiomyocyte Hypertrophy in *RAF1^{S257L/+}* iCMs

To identify the most likely targets for the hypertrophic phenotype in our *RAF1* mutant iCMs, we systematically analyzed several signaling pathways previously suggested to be causal to hypertrophy in response to elevated RAF1 activity. Cyclosporin A, a calcineurin inhibitor, has previously been proposed to prevent hypertrophy in rodent cardiomyocytes with ectopic overexpression of various *RAF1* mutants.²⁰ However, here, we did not observe significant reduction of hypertrophy in *RAF1^{S257L/+}* iCMs after treatment with cyclosporin A (10 $\mu\text{mol/L}$, 48 hours; Figure XIA and XIB in the online-only Data Supplement), despite an observed overall decreased activity in calcineurin in response to the inhibitor (Figure XIC in the online-only Data Supplement). In addition, although baseline nuclear factor of activated T cells transcriptional activity was increased in the *RAF1^{S257L/+}* iCMs compared with the *RAF1^{corr/+}* iCMs (Figure XID in the online-only Data Supplement), treatment with cyclosporin A had no effect on this baseline activity in either the *RAF1^{corr/+}* or the *RAF1^{S257L/+}* iCMs. Cyclosporin A reduced nuclear factor of activated T cells activity in *RAF1^{corr/+}* and *RAF1^{S257L/+}* iCMs, but only in response to induced calcineurin activity by phorbol 12-myristate 13-acetate and ionomycin (Figure XID in the online-only Data Supplement). Indeed, similar results on nuclear factor of activated T cells activity have previously been reported in neonatal rat cardiomyocytes overexpressing MEK1 or constitutively active *RAF1*.^{20,21} Taken together, our data demonstrate that activation of the NFAT cells pathway does not drive hypertrophy in *RAF1* mutant cardiomyocytes.

Because the AKT/mTOR pathway has also been previously implicated in RASopathy-associated hypertrophy,²² we next asked whether the activation of this

pathway could trigger hypertrophy in *RAF1^{S257L/+}* iCMs. Activation of AKT or its downstream effectors, PRAS40 and GSK3, was unchanged in mutant cells compared with controls (Figure XIIA through XIID in the online-only Data Supplement). Similarly, activation of mTOR (Figure XIIA and XIIB in the online-only Data Supplement) and its downstream targets, ribosomal S6 (Figure XIIA and XIIB in the online-only Data Supplement) or Eif4E (Figure XIIE and XIIF in the online-only Data Supplement), was not modified by expression of the *RAF1^{S257L/+}* mutation in iCMs.

Finally, we also did not observe changes in activation of p38 or JNK MAPK signaling (Figure XIIG through XIJ in the online-only Data Supplement). Taken together, our data indicate that hypertrophy of *RAF1^{S257L/+}* iCMs is not mediated by an increase in AKT/mTOR, p38, or JNK signaling pathways.

MEK5-ERK5 Activation Promotes Hypertrophy in *RAF1^{S257L/+}* iCMs

Although U0126 is defined primarily as a MEK1/2 inhibitor,¹⁹ several reports have demonstrated that, even at low doses (and contrary to PD98059 and trametinib), U0126 also inhibits MEK5-ERK5 signaling by targeting MEK5 activity,²³ suggesting that inhibition of MEK5-ERK5 could underlie the unexpected capacity of U0126 to reduce *RAF1^{S257L/+}* iCM surface area. To test whether activation of the MEK5-ERK5 pathway might be responsible for the hypertrophic phenotype in *RAF1^{S257L/+}* iCMs, we specifically inhibited this pathway with BIX02189, a highly potent and specific inhibitor of both MEK5 ($\text{IC}_{50}=1.5 \text{ nmol/L}$) and ERK5 ($\text{IC}_{50}=59 \text{ nmol/L}$) that has no affinity to *RAF1*, ERK1/2, or MEK1/2, even at high concentrations ($>100 \mu\text{mol/L}$).²⁴ We found that treatment of *RAF1^{S257L/+}* iCMs with BIX02189 significantly reduced cell surface area (Figure 6A and 6B), indicating that the MEK5-ERK5 signaling pathway may be responsible for the hypertrophy in *RAF1* mutant iCMs. BIX02189 did not affect *RAF1^{corr/+}* iCM size (Figure 6A and 6B), indicating that MEK5-ERK5 signaling is not required for normal cardiomyocyte homeostasis. At the structural level, and like U0126, inhibition of the MEK5-ERK5 pathway did not ameliorate myofibrillar disarray (Figure 6C and 6D). Treatment with both BIX02189 and PD98059, however, improved the *RAF1^{S257L/+}* iCMs structure (Figure 6C and 6D) to levels similar to those of PD98059 treatment alone, suggesting that the effects of either inhibitor are not additive but rather specific to its targeted signaling pathway.

To further validate these results, we expressed a dominant negative ERK5 by transducing *RAF1^{S257L/+}* iCMs with Ad-dominant negative ERK5 (Figure XIII A in the online-only Data Supplement) and found that it reduced cardiac cell size (Figure XIII B and XIII C in the online-only Data Supplement) but did not improve

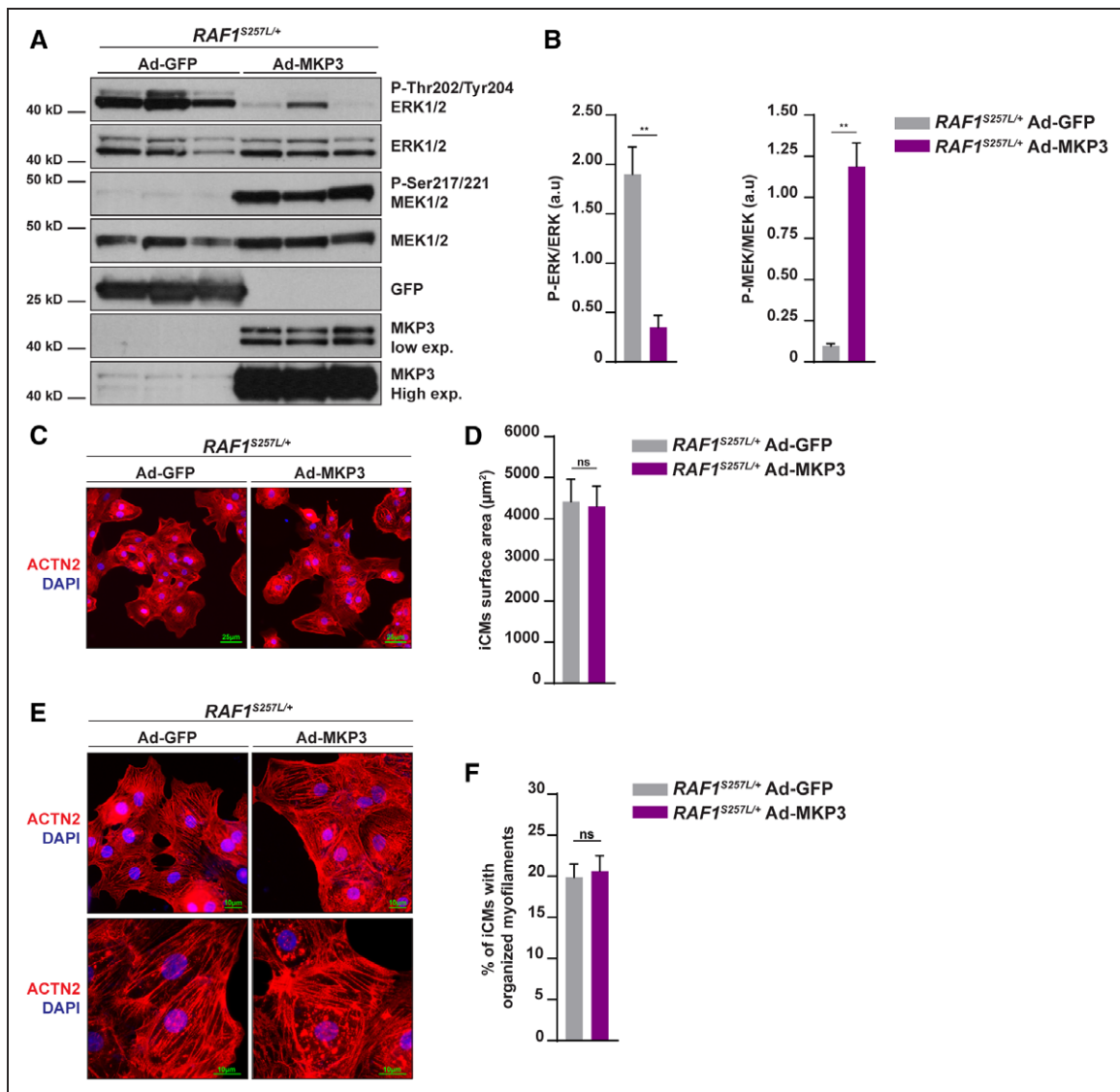


Figure 5. Specific inhibition of extracellular regulated kinase 1/2 (ERK1/2) activation with Ad-MAPK phosphatase 3 (MKP3) has no effect on *RAF1*^{S257L/+} inducible pluripotent stem cell-derived cardiomyocyte (iCM) hypertrophy.

A, Western blot of phospho-ERK1/2, ERK1/2, phospho-mitogen-activated protein kinase kinase 1/2 (MEK1/2), MEK1/2, MKP3, and green fluorescent protein (GFP) levels in mutant iCMs infected with 20 multiplicity of infection (MOI) Ad-GFP or Ad-MKP3. Each lane represents 1 independent differentiation of each lineage. **B**, Quantification of ERK1/2 and MEK1/2 level of activation. Phospho-ERK1/2 levels were normalized to total ERK1/2. Phospho-MEK1/2 levels were normalized to total MEK1/2. (n=3). **C**, Representative immunofluorescence images of mutant iCMs infected with 20 MOI of Ad-GFP or Ad-MKP3 and immunostained for ACTN2 and DAPI. **D**, Quantification of iCM surface area of *RAF1*^{S257L/+} iCMs infected with Ad-GFP or Ad-MKP3 obtained from 3 independent differentiations (n=3). For each independent experiment, 7 to 10 immunofluorescence images were taken randomly for each well of each transduction (representing 200–300 iCMs measured per independent experiment). **E**, Representative images of myofilament organization in *RAF1*^{S257L/+} iCMs infected with Ad-GFP or Ad-MKP3 shown by immunofluorescence staining for ACTN2 and DAPI. **F**, Quantification of *RAF1*^{S257L/+} iCMs with organized myofilaments (n=3). For each independent experiment, 7 to 10 immunofluorescence images were taken randomly for each well of each condition (representing 100–300 iCMs). Results are presented as mean±SEM. **P*<0.05. ***P*<0.01. a.u. indicates arbitrary units; and ns, nonsignificant.

myofibrillar structure (Figure XIID and XIIE in the online-only Data Supplement). This finding confirms that the *RAF1*^{S257L/+} mutation elicits hypertrophy specifically through activation of the ERK5 signaling pathway.

MEK5 and ERK5 were not previously thought to be targets of RAF1 kinase activity.²⁵ Accordingly, neither differences in phosphorylation of ERK5 at the TEY site (Thr218/Tyr220) nor variations in the overall electrophoretic mobility (phosphorylation shift) of ERK5 were observed between *RAF1*^{S257L/+} and *RAF1*^{corr/+} iCMs

(Figure XIIF and XIIG). However, because ERK5 activity, defined by its capacity to activate downstream effectors, does not always correlate with its kinase activity or its phosphorylation status,²⁶ we also measured MEF2 transcriptional activity, a major downstream target of MEK5-ERK5. In this regard, we found that MEF2 activity was significantly increased in *RAF1*^{S257L/+} iCMs and that inhibition of MEK5-ERK5 signaling with BIX02189 drastically reduced MEF2 activity (Figure 6E). We observed a similar increase in MEF2 activity in *RAF1*^{S257LIntr.+/+} iCMs

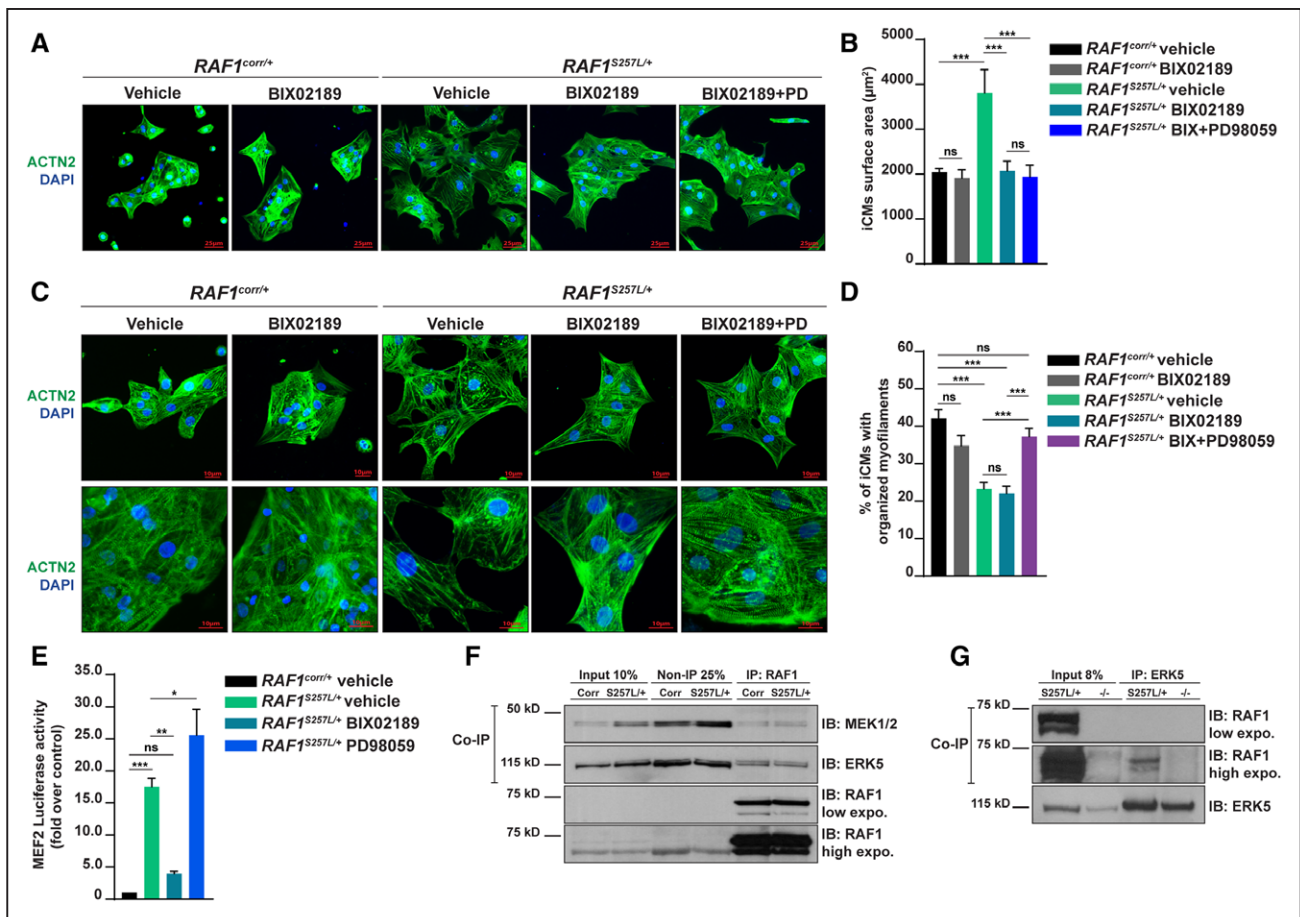


Figure 6. Mitogen-activated protein kinase kinase (MEK) 5–extracellular regulated kinase 5 (ERK5) pathway inhibition prevents hypertrophy in *RAF1*^{S257L/+} cardiomyocytes.

A, Representative immunofluorescence images and cell surface area quantification (**B**) of isogenic *RAF1*^{corr/+} or *RAF1*^{S257L/+} inducible pluripotent stem cell–derived cardiomyocytes (iCMs; Actinin Alpha 2 [ACTN2] and 4',6-diamidino-2-phenylindole [DAPI] positive) treated for 48 hours with vehicle or the MEK5-ERK5 inhibitor BIX02189 (25 μmol/L). Results were obtained from 3 independent differentiations (n=3). For each independent experiment, 7 to 10 immunofluorescence images were taken randomly for each well of each condition (representing 200–300 iCMs measured per independent experiment). **C**, Representative images of myofilament organization in isogenic *RAF1*^{corr/+} or *RAF1*^{S257L/+} iCMs and percentage of iCMs with organized myofilaments (**D**) in isogenic *RAF1*^{corr/+} or *RAF1*^{S257L/+} iCMs treated for 48 hours with vehicle or the MEK5-ERK5 inhibitor BIX02189 (25 μmol/L). Results were obtained from 3 independent differentiations (n=3). For each independent experiment, 7 to 10 immunofluorescence images were taken randomly for each well (representing 100–300 iCMs per independent experiment). **E**, MEF2 luciferase activity in isogenic *RAF1*^{corr/+} treated with vehicle or *RAF1*^{S257L/+} iCMs treated for 48 hours with vehicle, BIX02189 (25 μmol/L), or PD98059 (25 μmol/L). Results were obtained from 3 independent differentiations (n=3). Results are represented as mean±SEM. **P*<0.05. ***P*<0.01. ****P*<0.001. **F**, *RAF1*^{corr/+} or *RAF1*^{S257L/+} iCMs lysates were immunoprecipitated with an anti-RAF1 antibody. The input, the nonbound fractions, and the bound fractions were immunoblotted with the indicated antibodies. MEK1/2 (45–47 kDa) and ERK5 (115 kDa) were coimmunoprecipitated with RAF1 in iCMs. **G**, *RAF1*^{S257L/+} or *RAF1*^{-/-} lysates were immunoprecipitated with an anti-ERK5 antibody. The input and the bound fractions were immunoblotted with the indicated antibodies. RAF1 (74 kDa) was coimmunoprecipitated with ERK5 only in mutant iCMs. Corr indicates corrected cells; expo, exposure; IB, immunoblot; IP, immunoprecipitation; and ns, nonsignificant.

(Figure VK in the online-only Data Supplement). The PD98059 inhibitor led to a slight but significant increase in MEF2 activity, suggesting that the MEK1/2-ERK1/2 pathway negatively regulates MEF2 activity in mutant iCMs (Figure 6E).

To determine the mechanism by which RAF1 modulates ERK5 signaling, we tested whether RAF1 might bind to and interact with ERK5 in iCMs. We performed a coimmunoprecipitation assay and found that RAF1 complexes with MEK1/2 and ERK5, with the same affinity in both *RAF1*^{S257L/+} and *RAF1*^{corr/+} iCMs (Figure 6F). This observed RAF1 coimmunoprecipitation is specific; we observed the complex between RAF1 and ERK5 only in *RAF1*^{S257L/+} iCMs, not in *RAF1*^{-/-} iCMs (Figure 6G).

Because ERK5 can be differentially localized to either the cytosol or nucleus, we next investigated whether *RAF1*^{S257L/+} could influence ERK5 localization. We found that although ERK5 localized predominantly to the nucleus in both *RAF1*^{S257L/+} and *RAF1*^{corr/+} iCMs (Figure XIIIH in the online-only Data Supplement), its localization was significantly augmented in the mutant iCMs (Figure XIIIH and XIII), suggesting that *RAF1*^{S257L/+} may increase ERK5 transcriptional activity by enhancing its nuclear translocation. Taken together, these data are the first to identify that aberrant regulation of the MEK5-ERK5 pathway leads to a hypertrophic phenotype in *RAF1*-associated NS.

Identification of Genes With Deregulated Expression in *RAF1*^{S257L/+} iCMs

Although several studies have uncovered abnormal signaling pathways in RASopathy disorders, little is known about the alterations of the cardiac transcriptome induced by NS mutations. Hence, to gain insights into the transcriptional alterations induced by the NS-associated *RAF1*^{S257L/+} mutation in human cardiomyocytes, we performed quantitative transcriptome profiling by RNA-sequencing, which revealed 150 differentially expressed genes (false discovery rate <0.05) in mutant versus isogenic *RAF1*^{corr/+} iCMs, of which 85 were upregulated and 65 were downregulated (Figure 7A and Table V in the online-only Data Supplement). We validated these findings by reverse transcriptase–quantitative PCR analysis of a subset of the top upregulated or downregulated genes (Figure 7B and 7C).

The most upregulated gene in mutant iCMs was the recently uncovered long non-coding RNA (lncRNA) *LOC100128252* or *MORT*²⁷ (Figure 7A and Table V in the online-only Data Supplement). Its function remains elusive, but *MORT* expression has been shown to be epigenetically silenced in many human cancers, suggesting that *MORT* mediates control of cellular proliferation.²⁷ Hence, increased expression of *MORT* in NS iCMs could be the result of a negative feedback regulation of proliferation, mediated by the sustained activation of the MEK1/2-ERK1/2 signaling pathway in *RAF1*^{S257L/+} mutant cells. RNA-sequencing also revealed that *HAND1*, *HEY2*, and *TBX20*, 3 critical cardiac transcription factors crucial for cardiac development, were significantly downregulated in mutant iCMs (Figure 7A and 7B and Table V in the online-only Data Supplement).

RAF1^{S257L/+} Dysregulates Sarcomeric and Extracellular Matrix Gene Expression in Cardiomyocytes

To determine the relationship between gene expression alteration and phenotypic change, we used gene ontology analysis to rank enriched biological processes in mutant iCMs. We found that *RAF1*^{S257L/+} disrupted expression of genes involved in ErbB receptor signaling (*ERBB2/4*, *NRG1*, *AREG*; Figure 7D and Table V in the online-only Data Supplement), an essential pathway critical for trabeculae formation during cardiac development.²⁸ In addition, genes involved in HCM or dilated cardiomyopathy were dysregulated as well, suggesting that transcriptional alteration in genes involved with sarcomeric structure such as *MYH7*, *TNNC1*, *ACTG1*, *TNNT2*, *TPM1*, or *MYBPC3* (Figure 7D and Table V in the online-only Data Supplement) contribute to the abnormal myofibrillar phenotype of *RAF1*^{S257L/+} iCMs. Similarly, we also found strong enrichment of genes involved in regulation of extracellular matrix (ECM)

homeostasis (*COL8A1*, *MMPs*, *ADAMTS9*), laminin interactions (*LAMA2*, *NID2*), or focal adhesion (*THBS1*, *LAMA4*; Figure 7D and Table V in the online-only Data Supplement), which may be involved in the hypertrophy phenotype of these cells.

We next identified the gene transcriptional profiles that were specifically affected by either MEK5-ERK5 or MEK1/2-ERK1/2 activation in *RAF1*^{S257L/+} iCMs. To do this, we examined genes with an expression that was altered in mutant *RAF1*^{S257L/+} iCMs but normalized after either BIX02189 or PD98059 treatment. We found that among the 150 genes dysregulated in mutant cells, 15 were specifically altered by the ERK5 inhibitor, 14 of which became normalized to levels similar to that of control isogenic iCMs (Figure 7E and Table VI in the online-only Data Supplement). Specifically, BIX02189, which reduced *RAF1*^{S257L/+} iCM size, normalized the mRNA expression of several ECM genes such as *COL8A1*, *ADAMTS9*, *HAPLN1*, or *TINAGL1* (Figure 7F). In addition, expression of *SMPX*, a protein that localizes to the costameric cytoskeleton of muscle cells to regulate cytoskeletal dynamics,²⁹ was normalized by BIX02189 (Figure 7F).

Surprisingly, the number of genes normalized specifically by the MEK1/2 inhibitor was more limited (Figure 7G and Table VII in the online-only Data Supplement). PD98059 reduced or normalized the expression of genes known to regulate actin polymerization such as *DOCK11*, a positive activator of CDC42,³⁰ and *TMSB4X*, one of the main intracellular actin sequestering factors.³¹ These data suggest that activation of the MEK1/2-ERK1/2 pathway alters actin filament dynamics, likely accounting for the myofiber disarray phenotype observed in *RAF1*^{S257L/+} iCMs. Moreover, expression of *CYR61*, a ligand of integrin receptors,³² was also normalized by PD98059 (Figure 7G and Table VII in the online-only Data Supplement). Hence, because integrin receptors connect the ECM to the sarcomere,³³ abnormal levels of *CYR61* could also participate in the development of myofibrillar disarray in the mutant iCMs.

Taken together, our data reveal that NS *RAF1*^{S257L/+} elicits HCM through aberrant activation of both MEK5-ERK5 and MEK1/2 pathways in human cardiomyocytes, driving hypertrophy and myofibrillar disarray, respectively (Figure 7H). At the transcriptional level, we identified defined subsets of genes downstream of MEK1/2 or ERK5 involved in sarcomeric structure and ECM homeostasis that could contribute to the NS-associated HCM phenotype.

DISCUSSION

We generated iCMs from an NS *RAF1*^{S257L/+} patient with HCM and developed control lines using genome editing. Mutant iCMs phenocopy the hypertrophic pathology (increased cell surface area, myofibrillar disarray)

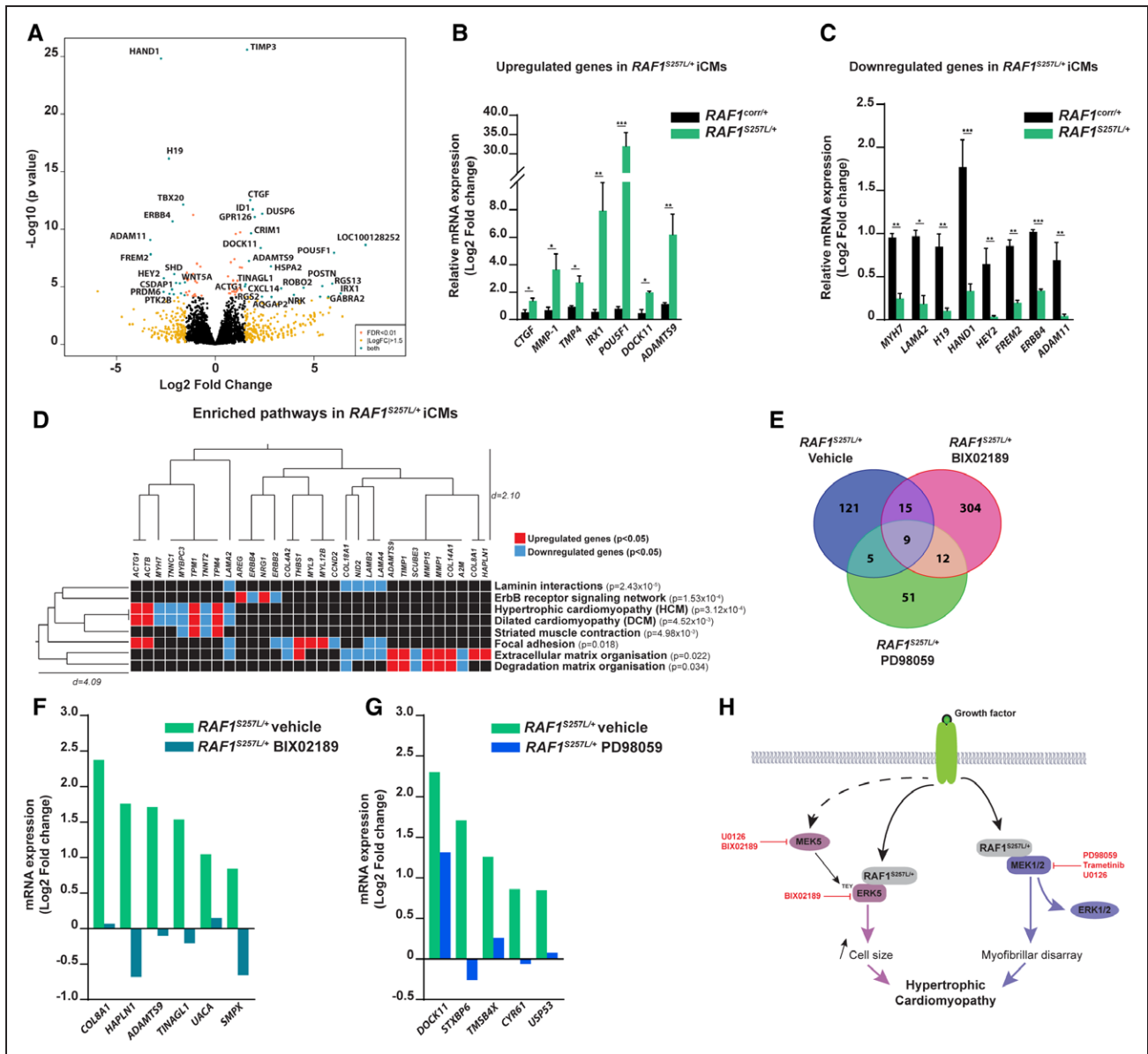


Figure 7. *RAF1^{S257L/+}* deregulates mRNA expression of genes necessary for cardiac development, extracellular matrix, and cytoskeleton homeostasis in cardiomyocytes.

A, Volcano plot showing the top 40 differentially expressed genes between isogenic *RAF1^{ctrl/+}* and *RAF1^{S257L/+}* in inducible pluripotent stem cell-derived cardiomyocytes (iCMs). Green dots represent genes differentially expressed with a false discovery rate <math><0.01</math> and log fold change > 1.5 (n=3 for each group). **B**, Reverse transcriptase–quantitative polymerase chain reaction (RT-qPCR) validation of a representative subset of upregulated genes identified by RNA-sequencing in *RAF1^{S257L/+}* iCMs (n=3). Results are presented as mean±SEM. *C, RT-qPCR validation of a representative subset of downregulated genes by RNA-sequencing in *RAF1^{S257L/+}* iCMs (n=3). Results are presented as mean±SEM. *D, Gene ontology enrichment analysis depicting the significantly enriched pathways (RAF1^{S257L/+} iCMs. **E**, Venn diagram indicating the number of genes deregulated in *RAF1^{S257L/+}* iCMs (blue circle) that are significantly (F, Genes upregulated in *RAF1^{S257L/+}* vs isogenic *RAF1^{ctrl/+}* iCMs that are significantly normalized only by BIX02189 (G, Genes upregulated in *RAF1^{S257L/+}* vs isogenic *RAF1^{ctrl/+}* iCMs that are significantly normalized only by PD98059 (H, Proposed model illustrating the signaling pathways that underlie NS *RAF1^{S257L/+}*-associated HCM. *RAF1^{S257L/+}* drives HCM by coactivating the mitogen-activated protein kinase kinase (MEK) 1/2 and extracellular regulated kinase (ERK) 5 signaling pathways in human cardiomyocytes. *RAF1^{S257L/+}* triggers activation of the MEK1/2 pathway, which impairs sarcomeric homeostasis. In addition, *RAF1^{S257L/+}* elicits activation of the ERK5 pathway, which elicits increased cardiomyocyte size.

observed in human patients. Moreover, although MEK1/2 signaling is aberrant in *RAF1^{S257L/+}* iCMs, leading to abnormal organization of the sarcomere, it is the cell-autonomous activation of the MEK5-ERK5 pathway that elicits the cardiomyocyte hypertrophy in *RAF1^{S257L/+}*-associated NS. In this regard, inhibition of MEK1/2, but

not ERK1/2, reversed the sarcomeric disarray in these iCMs, whereas, conversely, inhibition of MEK5-ERK5 reversed the hypertrophic phenotype. Finally, using RNA-sequencing, we uncovered that mutant iCMs display altered expression of several genes essential for cardiac development, sarcomeric function, and ECM

homeostasis. Of these, we identified several ECM and cytoskeletal regulatory genes that were dysregulated by hyperactivation of ERK5, whereas genes involved in actin dynamic regulation were altered in response to hyperactivation of MEK1/2-ERK1/2 signaling.

Our study is the first to reveal that MEK5-ERK5 signaling is abnormally activated in NS-associated RAF1 mutations, suggesting that its activation is a key driver for cardiomyocyte hypertrophy in these patients. These data agree with previous studies showing that aberrant ERK5-MEF2 activity induces cardiac hypertrophy.³⁴ Our study shows that *RAF1*^{S257L/+} iCMs have deregulated expression of ECM genes, which are normalized by BIX02189, a specific inhibitor of the MEK5-ERK5 pathway. These data suggest that increased expression of ECM and cytoskeletal network genes in RAF1 mutant iCMs may be causal to the increased cell size phenotype in *RAF1*^{S257L/+} NS.

RAF1^{S257L/+} does not increase ERK5 activity by phosphorylation of its TEY site of the kinase domain or other regions of ERK5 known to be important for kinase activity. It was previously suggested that RAF1 forms a complex with ERK5 in HEK293 cells.³⁵ Although RAF1 does not phosphorylate ERK5 directly, it is conceivable that RAF1 serves as a scaffold to stabilize ERK5 conformation and to promote translocation to the nucleus, particularly because ERK5 retains its transcriptional activity even in its kinase-inactive form.²⁶ Exactly how NS-associated RAF1 mutations enhance ERK5 nuclear localization remains to be investigated.

Both RAF1 and ERK5 can localize to the nucleus.^{36,37} RAF1 can translocate to the nucleus in response to growth factor stimulation,³⁶ but because it lacks a nuclear localization sequence, its mechanism of translocation remains unclear. Unlike RAF1, however, ERK5 contains a nuclear localization sequence, which is unmasked on phosphorylation of its TEY site by MEK5 (prevented by BIX02189, U0126, or dominant negative ERK5), allowing ERK5 autophosphorylation and translocation into the nucleus, where it can induce gene transcription. In addition, it is possible that ERK5 is a protein chaperone, allowing RAF1 to translocate to the cardiomyocyte nucleus, where gain-of-function RAF1 might mediate hyperphosphorylation of downstream nuclear targets that trigger transcriptional activation of hypertrophic genes.

Our data confirm that cyclosporin A efficiently inhibits calcineurin activity in iCMs (Figure XIC in the online-only Data Supplement) but that calcineurin signaling is not the primary pathway driving the increased cell size in *RAF1*^{S257L/+} iCMs. Contrary to Dhandapany et al,²⁰ we show that calcineurin does not mediate hypertrophy in *RAF1*^{S257L/+} iCMs. In their experiments, Dhandapany et al overexpressed *RAF1* wild-type and *RAF1* S257L in rat cardiomyocytes and used ³H leucine incorporation as a readout for cardiomyocyte hypertrophy; they did

not directly report cell size or structural organization in *RAF1* S257L-overexpressed cells. Moreover, they reported similar increases in ³H leucine incorporation between *RAF1* wild-type and *RAF1* S257L-overexpressed myocytes and a similar reduction in ³H leucine incorporation after cyclosporin A treatment between *RAF1* wild-type and S257L cells, suggesting that cyclosporin A reduced increased translation/protein synthesis when RAF1 is overexpressed, independently of the *RAF1* mutation. Indeed, cyclosporin A has been shown to alter protein synthesis in various organs, including kidneys, heart, and liver.³⁸

Strikingly, although U0126, PD98059, trametinib, and Ad-MKP3 all reduced ERK1/2 phosphorylation, only PD98059 and trametinib rescued myofiber disarray in the *RAF1*^{S257L/+} iCMs. Although the inhibitors all bind MEK1/2, U0126 binds activated MEK1/2 specifically,^{18,19} thereby inhibiting MEK1/2-dependent phosphorylation of ERK1/2. In contrast, PD98059 and trametinib bind inactive MEK1/2, directly preventing MEK1/2 activation by RAF.^{18,19} Hence, this suggests that hyperactivation of MEK1/2 underlies the myofibril disarray in *RAF1*^{S257L/+} iCMs, a possibility reinforced by the absence of structural improvement in the mutant iCMs by treatment with Ad-MKP3, which targets only phosphorylated ERK1/2. Moreover, all 3 inhibitors also reduced MEK1/2 expression in *RAF1*^{S257L/+} iCMs, suggesting that additional regulatory mechanisms are required to modulate these signaling enzymes. ERK1/2 and MEK1/2 are known to associate directly with cytoskeletal molecules, including actin fibers,³⁹ intermediate filaments,⁴⁰ and tubulin microtubules,⁴¹ and to localize in the sarcomere, where MEK1/2-ERK1/2 can phosphorylate the N2B domain of titin,⁴² suggesting that MEK1/2 activity, independently of ERK1/2, may regulate myofilament homeostasis at the transcriptional and posttranscriptional levels. Further studies are required to delineate these molecular mechanisms.

Besides HCM, patients with NS *RAF1* display other congenital heart defects.⁶ Our RNA-sequencing data suggest that congenital heart defects in NS could be caused by altered expression of genes central to cardiac development such as *HAND1*, *HEY2*, or *TBX20*. Indeed, mice with targeted deletions of any one of these factors exhibited atrial septal defect or ventricular septal defect.^{43–45} Moreover, loss-of-function mutations in *HAND1*, *HEY2*, or *TBX20* are associated with severe septation defects in humans.^{46–48} Left ventricular non-compaction has recently been documented in patients with NS,⁴⁹ which might be mediated, at least in part, by decreased expression of *ERBB2* and *ERBB4*,²⁸ as was observed in our *RAF1*^{S257L/+} iCMs. However, the inhibition of MEK5-ERK5 or MEK1/2 did not rescue the aberrant downregulation of these cardiac developmental genes, suggesting that other as yet unknown signaling pathways could control their expression in *RAF1*^{S257L/+} iCMs.

CONCLUSIONS

Our iPSC-based disease modeling platform identifies that HCM in *RAF1*^{S257L/+} human iCMs is concomitantly driven by activation of both ERK5 and MEK1/2 signaling to induce increased cell size and myofibrillar disarray, respectively (Figure 7H). Combining ERK5 and MEK1/2 inhibitors may better treat severe NS-associated *RAF1*^{S257L/+} HCM. Whether targeting MEK5-ERK5 could also prevent hypertrophy in patients with other HCM-associated diseases remains to be determined. However, systemic injection of the MEK1/2 inhibitor PD0325901 in mice carrying a mutation in the CR3 domain of *RAF1* (*RAF1*^{L613V/+}) prevented HCM, suggesting that activation of the MEK1/2-ERK1/2 pathway underlies the phenotype.⁸ Because PD0325901 also inhibits MEK5 activity,⁵⁰ we speculate that *RAF1* mutations localized to the CR3 domain may also elicit hypertrophy via activation of MEK5-ERK5 signaling. Future work will delineate the nature of the *RAF1* and ERK5 interaction and decipher the exact function of MEK1/2 in the regulation of cardiomyocyte structural organization. We will also investigate whether the effects of the *RAF1*^{S257L/+} mutation in noncardiomyocyte cells of the heart such as fibroblasts, endothelial cells, or smooth muscle cells contribute to the severity of the HCM in these patients.

ARTICLE INFORMATION

Received August 4, 2018; accepted April 11, 2019.

The online-only Data Supplement is available with this article at <https://www.ahajournals.org/doi/suppl/10.1161/circulationaha.118.037227>.

Correspondence

Fabrice Jaffré, PhD, Weill Cornell Medical College, Department of Surgery, Cornell University, New York, NY 10065; or Maria Irene Kontaridis, PhD, Masonic Medical Research Institute, 2150 Bleecker St, Utica, NY 13501. Email faj4001@med.cornell.edu, mkontaridis@mmri.edu, or mkontari@bidmc.harvard.edu

Affiliations

Department of Medicine, Division of Cardiology, Beth Israel Deaconess Medical Center (F.J., M.I.K.), Department of Biological Chemistry and Molecular Pharmacology (M.I.K.), Harvard Medical School, Boston, MA (F.J., M.I.K.). Department of Surgery, Weill Cornell Medical College, New York, NY (F.J., T.E.). Center for Public Health Genomics, Department of Public Health Sciences, Biochemistry and Molecular Genetics, and Biomedical Engineering, University of Virginia, Charlottesville (C.L.M.). Institute of Neuropathology (A.S.), Department of Child Neurology (A.H.), University Hospital Giessen, Justus Liebig University Giessen, Germany. Department of Cardiology, Division of Genetics, Boston Children's Hospital, MA (A.E.R.). Harvard Stem Cell Institute, Harvard University, Cambridge, MA (M.I.K.). Masonic Medical Research Institute, Utica, NY (M.I.K.).

Acknowledgments

The authors thank the family for their collaboration. They thank the Human Neuron Differentiation Services at the Human Neuron Core at Boston Children's Hospital for performing the RNA-sequencing. They also thank the Rockefeller University Flow Cytometry Resource Center for performing cell size measurement with the Amnis ImageStream-X image analyzer. In addition, they thank Dr William T. Pu at Boston Children's Hospital for providing training in iPSC reprogramming and culture. F.J. and M.I.K. designed the study. F.J. performed the majority of the experiments, analyzed the data, generated figures, and drafted the manuscript. C.L.M. performed the RNA-sequencing data analyses. A.S. performed the cardiac tissue histology experiments. A.R. provided expertise in NS

phenotype/genotype correlations. A.H. provided the human pediatric dermal cells and the patient clinical data. T.E. provided critical feedback. M.I.K. oversaw the project, data acquisition, and analyses and participated in the manuscript preparation, writing, and editing.

Sources of Funding

This work was supported by the National Institutes of Health (grants R01-HL114775, R01-HL122238, R01-HL102368), the Harvard Stem Cell Institute (seed grant), the Saving Tiny Hearts Foundation, and the Beth Israel Deaconess Medical Center Department of Medicine, Division of Cardiology to Dr Kontaridis; a National Institutes of Health Pathway to Independence grant (R00 HL12592) to Dr Miller; grants from the National Institutes of Health (R35-HLHL135778) and Department of Defense (W81XWH-17-1-0661) to Dr Evans; and a Scientist Development Grant from the American Heart Association (16SDG30580000) and the Canadian Rare Disease Foundation to Dr Jaffré.

Disclosures

None.

REFERENCES

- Roberts AE, Allanson JE, Tartaglia M, Gelb BD. Noonan syndrome. *Lancet*. 2013;381:333–342. doi: 10.1016/S0140-6736(12)61023-X
- Chen PC, Yin J, Yu HW, Yuan T, Fernandez M, Yung CK, Trinh QM, Peltekova VD, Reid JG, Tworog-Dube E, Morgan MB, Muzny DM, Stein L, McPherson JD, Roberts AE, Gibbs RA, Neel BG, Kucherlapati R. Next-generation sequencing identifies rare variants associated with Noonan syndrome. *Proc Natl Acad Sci USA*. 2014;111:11473–11478. doi: 10.1073/pnas.1324128111
- Wilkinson JD, Lowe AM, Salbert BA, Sleeper LA, Colan SD, Cox GF, Towbin JA, Connuck DM, Messere JE, Lipshultz SE. Outcomes in children with Noonan syndrome and hypertrophic cardiomyopathy: a study from the Pediatric Cardiomyopathy Registry. *Am Heart J*. 2012;164:442–448. doi: 10.1016/j.ahj.2012.04.018
- Wellbrock C, Karasariades M, Marais R. The RAF proteins take centre stage. *Nat Rev Mol Cell Biol*. 2004;5:875–885. doi: 10.1038/nrm1498
- Romano D, Matallanas D, Weitsman G, Preisinger C, Ng T, Kolch W. Proapoptotic kinase MST2 coordinates signaling crosstalk between RASSF1A, Raf-1, and Akt. *Cancer Res*. 2010;70:1195–1203. doi: 10.1158/0008-5472.CAN-09-3147
- Razzaque MA, Nishizawa T, Komoike Y, Yagi H, Furutani M, Amo R, Kamisago M, Momma K, Katayama H, Nakagawa M, Fujiwara Y, Matsushima M, Mizuno K, Tokuyama M, Hirota H, Muneuchi J, Higashinakagawa T, Matsuoka R. Germline gain-of-function mutations in *RAF1* cause Noonan syndrome. *Nat Genet*. 2007;39:1013–1017. doi: 10.1038/ng2078
- Thompson D, Patrick-Esteve J, Surcouf JW, Rivera D, Castellanos B, Desai P, Lilje C, Lacassie Y, Marble M, Zambrano R. *RAF1* variants causing biventricular hypertrophic cardiomyopathy in two preterm infants: further phenotypic delineation and review of literature. *Clin Dysmorphol*. 2017;26:195–199. doi: 10.1097/MCD.0000000000000194
- Wu X, Simpson J, Hong JH, Kim KH, Thavarajah NK, Backx PH, Neel BG, Araki T. MEK-ERK pathway modulation ameliorates disease phenotypes in a mouse model of Noonan syndrome associated with the *Raf1*(L613V) mutation. *J Clin Invest*. 2011;121:1009–1025. doi: 10.1172/JCI44929
- Ran FA, Hsu PD, Lin CY, Gootenberg JS, Konermann S, Trevino AE, Scott DA, Inoue A, Matoba S, Zhang Y, Zhang F. Double nicking by RNA-guided CRISPR-Cas9 for enhanced genome editing specificity. *Cell*. 2013;154:1380–1389. doi: 10.1016/j.cell.2013.08.021
- Ran FA, Hsu PD, Wright J, Agarwala V, Scott DA, Zhang F. Genome engineering using the CRISPR-Cas9 system. *Nat Protoc*. 2013;8:2281–2308. doi: 10.1038/nprot.2013.143
- Lian X, Zhang J, Azarin SM, Zhu K, Hazeltine LB, Bao X, Hsiao C, Kamp TJ, Palecek SP. Directed cardiomyocyte differentiation from human pluripotent stem cells by modulating Wnt/ β -catenin signaling under fully defined conditions. *Nat Protoc*. 2013;8:162–175. doi: 10.1038/nprot.2012.150
- Rose BA, Force T, Wang Y. Mitogen-activated protein kinase signaling in the heart: angels versus demons in a heart-breaking tale. *Physiol Rev*. 2010;90:1507–1546. doi: 10.1152/physrev.00054.2009
- Burch M, Mann JM, Sharland M, Shinebourne EA, Patton MA, McKenna WJ. Myocardial disarray in Noonan syndrome. *Br Heart J*. 1992;68:586–588. doi: 10.1136/hrt.68.12.586

14. Cerrato F, Pacileo G, Limongelli G, Gagliardi MG, Santoro G, Digilio MC, Di Salvo G, Ardoriso R, Miele T, Calabrò R. A standard echocardiographic and tissue Doppler study of morphological and functional findings in children with hypertrophic cardiomyopathy compared to those with left ventricular hypertrophy in the setting of Noonan and LEOPARD syndromes. *Cardiol Young*. 2008;18:575–580. doi: 10.1017/S104795110800320X
15. Kobayashi T, Aoki Y, Niihori T, Cavé H, Verloes A, Okamoto N, Kawame H, Fujiwara I, Takada F, Ohata T, Sakazume S, Ando T, Nakagawa N, Lapunzina P, Meneses AG, Gillissen-Kaesbach G, Wieczorek D, Kurosawa K, Mizuno S, Ohashi H, David A, Philip N, Guliyeva A, Narumi Y, Kure S, Tsuchiya S, Matsubara Y. Molecular and clinical analysis of RAF1 in Noonan syndrome and related disorders: dephosphorylation of serine 259 as the essential mechanism for mutant activation. *Hum Mutat*. 2010;31:284–294. doi: 10.1002/humu.21187
16. Hüser M, Luckett J, Chiloeches A, Mercer K, Iwobi M, Giblett S, Sun XM, Brown J, Marais R, Pritchard C. MEK kinase activity is not necessary for Raf-1 function. *EMBO J*. 2001;20:1940–1951. doi: 10.1093/emboj/20.8.1940
17. Friday BB, Yu C, Dy GK, Smith PD, Wang L, Thibodeau SN, Adjei AA. BRAF V600E disrupts AZD6244-induced abrogation of negative feedback pathways between extracellular signal-regulated kinase and Raf proteins. *Cancer Res*. 2008;68:6145–6153. doi: 10.1158/0008-5472.CAN-08-1430
18. Alessi DR, Cuenda A, Cohen P, Dudley DT, Saitiel AR. PD 098059 is a specific inhibitor of the activation of mitogen-activated protein kinase kinase in vitro and in vivo. *J Biol Chem*. 1995;270:27489–27494. doi: 10.1074/jbc.270.46.27489
19. Favata MF, Horiuchi KY, Manos EJ, Daulerio AJ, Stradley DA, Feeser WS, Van Dyk DE, Pitts WJ, Earl RA, Hobbs F, Copeland RA, Magolda RL, Scherle PA, Trzaskos JM. Identification of a novel inhibitor of mitogen-activated protein kinase kinase. *J Biol Chem*. 1998;273:18623–18632. doi: 10.1074/jbc.273.29.18623
20. Dhandapanay PS, Fabris F, Tonk R, Illaste A, Karakikes I, Sorourian M, Sheng J, Hajjar RJ, Tartaglia M, Sobie EA, Lebeche D, Gelb BD. Cyclosporine attenuates cardiomyocyte hypertrophy induced by RAF1 mutants in Noonan and LEOPARD syndromes. *J Mol Cell Cardiol*. 2011;51:4–15. doi: 10.1016/j.yjmcc.2011.03.001
21. Sanna B, Bueno OF, Dai YS, Wilkins BJ, Molkentin JD. Direct and indirect interactions between calcineurin-NFAT and MEK1-extracellular signal-regulated kinase 1/2 signaling pathways regulate cardiac gene expression and cellular growth. *Mol Cell Biol*. 2005;25:865–878. doi: 10.1128/MCB.25.3.865-878.2005
22. Marin TM, Keith K, Davies B, Conner DA, Guha P, Kalaitzidis D, Wu X, Lauriol J, Wang B, Bauer M, Bronson R, Franchini KG, Neel BG, Kontaridis MI. Rapamycin reverses hypertrophic cardiomyopathy in a mouse model of LEOPARD syndrome-associated PTPN11 mutation. *J Clin Invest*. 2011;121:1026–1043. doi: 10.1172/JCI44972
23. Mody N, Leitch J, Armstrong C, Dixon J, Cohen P. Effects of MAP kinase cascade inhibitors on the MKK5/ERK5 pathway. *FEBS Lett*. 2001;502:21–24.
24. Tatake RJ, O'Neill MM, Kennedy CA, Wayne AL, Jakes S, Wu D, Kugler SZ Jr, Kashem MA, Kaplita P, Snow RJ. Identification of pharmacological inhibitors of the MEK5/ERK5 pathway. *Biochem Biophys Res Commun*. 2008;377:120–125. doi: 10.1016/j.bbrc.2008.09.087
25. English JM, Pearson G, Baer R, Cobb MH. Identification of substrates and regulators of the mitogen-activated protein kinase ERK5 using chimeric protein kinases. *J Biol Chem*. 1998;273:3854–3860. doi: 10.1074/jbc.273.7.3854
26. Erazo T, Moreno A, Ruiz-Babot G, Rodríguez-Asiain A, Morrice NA, Espadamala J, Bayasas JR, Gómez N, Lizcano JM. Canonical and kinase activity-independent mechanisms for extracellular signal-regulated kinase 5 (ERK5) nuclear translocation require dissociation of Hsp90 from the ERK5-Cdc37 complex. *Mol Cell Biol*. 2013;33:1671–1686. doi: 10.1128/MCB.01246-12
27. Vrba L, Garbe JC, Stampfer MR, Futscher BW. A lincRNA connected to cell mortality and epigenetically-silenced in most common human cancers. *Epigenerics*. 2015;10:1074–1083. doi: 10.1080/15592294.2015.1106673
28. Sanchez-Soria P, Camenisch TD. ErbB signaling in cardiac development and disease. *Semin Cell Dev Biol*. 2010;21:929–935. doi: 10.1016/j.semdb.2010.09.011
29. Schindeler A, Lavulo L, Harvey RP. Muscle costameric protein, Chisel/Smpx, associates with focal adhesion complexes and modulates cell spreading *in vitro* via a Rac1/p38 pathway. *Exp Cell Res*. 2005;307:367–380. doi: 10.1016/j.yexcr.2005.04.006
30. Lin Q, Yang W, Baird D, Feng Q, Cerione RA. Identification of a DOCK180-related guanine nucleotide exchange factor that is capable of mediating a positive feedback activation of Cdc42. *J Biol Chem*. 2006;281:35253–35262. doi: 10.1074/jbc.M606248200
31. Mannherz HG, Hannappel E. The beta-thymosins: intracellular and extracellular activities of a versatile actin binding protein family. *Cell Motil Cytoskeleton*. 2009;66:839–851. doi: 10.1002/cm.20371
32. Lau LF. CCN1/CYR61: the very model of a modern matricellular protein. *Cell Mol Life Sci*. 2011;68:3149–3163. doi: 10.1007/s00018-011-0778-3
33. Brancaccio M, Hirsch E, Notte A, Selvetella G, Lembo G, Tarone G. Integrin signalling: the tug-of-war in heart hypertrophy. *Cardiovasc Res*. 2006;70:422–433.
34. Kimura TE, Jin J, Zi M, Prehar S, Liu W, Oceandy D, Abe J, Neyses L, Weston AH, Cartwright EJ, Wang X. Targeted deletion of the extracellular signal-regulated protein kinase 5 attenuates hypertrophic response and promotes pressure overload-induced apoptosis in the heart. *Circ Res*. 2010;106:961–970. doi: 10.1161/CIRCRESAHA.109.209320
35. English JM, Pearson G, Hockenberry T, Shivakumar L, White MA, Cobb MH. Contribution of the ERK5/MEK5 pathway to Ras/Raf signaling and growth control. *J Biol Chem*. 1999;274:31588–31592. doi: 10.1074/jbc.274.44.31588
36. Geil WM, Yen A. Nuclear Raf-1 kinase regulates the CXCR5 promoter by associating with NFATc3 to drive retinoic acid-induced leukemic cell differentiation. *FEBS J*. 2014;281:1170–1180. doi: 10.1111/febs.12693
37. Gomez N, Erazo T, Lizcano JM. ERK5 and cell proliferation: nuclear localization is what matters. *Front Cell Dev Biol*. 2016;4:105. doi: 10.3389/fcell.2016.00105
38. Buss WC, Stepanek J. Tissue specificity of translation inhibition in Sprague-Dawley rats following in vivo cyclosporin A. *Int J Immunopharmacol*. 1993;15:775–782.
39. Leinweber BD, Leavis PC, Grabarek Z, Wang CL, Morgan KG. Extracellular regulated kinase (ERK) interaction with actin and the calponin homology (CH) domain of actin-binding proteins. *Biochem J*. 1999;344(pt 1):117–123.
40. Perlson E, Hanz S, Ben-Yaakov K, Segal-Ruder Y, Seger R, Fainzilber M. Vimentin-dependent spatial translocation of an activated MAP kinase in injured nerve. *Neuron*. 2005;45:715–726. doi: 10.1016/j.neuron.2005.01.023
41. Reszka AA, Segert R, Diltz CD, Krebs EG, Fischer EH. Association of mitogen-activated protein kinase with the microtubule cytoskeleton. *Cell Biol*. 1995;92:8881–8885.
42. Raskin A, Lange S, Banares K, Lyon RC, Ziesenis A, Lee LK, Yamazaki KG, Granzier HL, Gregorio CC, McCulloch AD, Omens JH, Sheikh F. A novel mechanism involving four-and-a-half LIM domain protein-1 and extracellular signal-regulated kinase-2 regulates titin phosphorylation and mechanics. *J Biol Chem*. 2012;287:29273–29284. doi: 10.1074/jbc.M112.372839
43. McFadden DG, Barbosa AC, Richardson JA, Schneider MD, Srivastava D, Olson EN. The Hand1 and Hand2 transcription factors regulate expansion of the embryonic cardiac ventricles in a gene dosage-dependent manner. *Development*. 2005;132:189–201. doi: 10.1242/dev.01562
44. Donovan J, Kordylewska A, Jan YN, Utset MF. Tetralogy of Fallot and other congenital heart defects in Hey2 mutant mice. *Curr Biol*. 2002;12:1605–1610.
45. Stennard FA, Costa MW, Lai D, Biben C, Furtado MB, Solloway MJ, McCulley DJ, Leimena C, Preis JI, Dunwoodie SL, Elliott DE, Prall OW, Black BL, Fatkin D, Harvey RP. Murine T-box transcription factor Tbx20 acts as a repressor during heart development, and is essential for adult heart integrity, function and adaptation. *Development*. 2005;132:2451–2462. doi: 10.1242/dev.01799
46. Kirk EP, Sunde M, Costa MW, Rankin SA, Wolstein O, Castro ML, Butler TL, Hyun C, Guo G, Otway R, Mackay JP, Waddell LB, Cole AD, Hayward C, Keogh A, Macdonald P, Griffiths L, Fatkin D, Sholler GF, Zorn AM, Feneley MP, Winlaw DS, Harvey RP. Mutations in cardiac T-box factor gene TBX20 are associated with diverse cardiac pathologies, including defects of septation and valvulogenesis and cardiomyopathy. *Am J Hum Genet*. 2007;81:280–291. doi: 10.1086/519530
47. Reamon-Buettner SM, Borlak J. HEY2 mutations in malformed hearts. *Hum Mutat*. 2006;27:118. doi: 10.1002/humu.9390
48. Reamon-Buettner SM, Ciribilli Y, Traverso I, Kuhls B, Inga A, Borlak J. A functional genetic study identifies HAND1 mutations in septation defects of the human heart. *Hum Mol Genet*. 2009;18:3567–3578. doi: 10.1093/hmg/ddp305
49. Hinton RB, Goldenberg P, Godby RC, Parrott A, Shikany AG, Landis BJ, James JF, Miller EM, Ware SM. Left ventricular noncompaction in Noonan syndrome. *J Genet Disor Genet Rep*. 2016;5:2.
50. Bain J, Plater L, Elliott M, Shpiro N, Hastie CJ, McLaughlan H, Klevernic I, Arthur JS, Alessi DR, Cohen P. The selectivity of protein kinase inhibitors: a further update. *Biochem J*. 2007;408:297–315. doi: 10.1042/BJ20070797